Structural Engineering Report No. 74

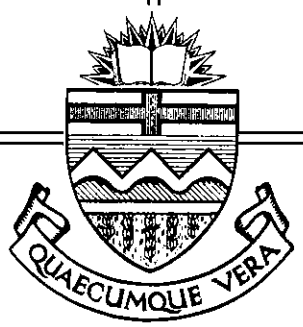

AN EFFECTIVE UNIAXIAL TENSILE STRESS-STRAIN RELATIONSHIP FOR PRESTRESSED CONCRETE

By
L. CHITNUYANONDH
S. RIZKALLA
D. W. MURRAY
J. G. MacGREGOR

February 1979

RECENT STRUCTURAL ENGINEERING REPORTS

Department of Civil Engineering

University of Alberta

45. *Ultimate Strength of Continuous Composite Beams* by S. Hamada and J. Longworth, August 1973.

46. *Prestressed Concrete I-Beams Subjected to Combined Loadings* by D.L.N. Rao and J. Warwaruk, November 1973.

47. *Finite Element Analysis for Combined Loadings with Improved Hexahedrons* by D.L.N. Rao and J. Warwaruk, November 1973.

48. *Solid and Hollow Rectangular Prestressed Concrete Beams Under Combined Loading* by J. Misic and J. Warwaruk, September 1974.

49. *The Second-Order Analysis of Reinforced Concrete Frames* by S.E. Hage and J.G. MacGregor, October 1974.

50. *Web Slenderness Limits for Compact Beam-Columns* by M.J. Perlynn and G.L. Kulak, September 1974.

51. *Web Slenderness Limits for Non-Compact Beams* by N.M. Holtz and G.L. Kulak, August 1975.

52. *Decision Table Processing of the Canadian Standards Association Specification S16.1* by S.K.F. Wu and D.W. Murray, February 1976.

53. *Web Slenderness Limits for Non-Compact Beam-Columns* by D.S. Nash and G.L. Kulak, March 1976.

54. *A Monte Carlo Study of the Strength Variability of Rectangular Tied Reinforced Concrete Columns* by L.H. Grant and J.G. MacGregor, March 1976.

55. *An Elastic Stress Analysis of a Gentilly Type Containment Structure - Volume 1* by D.W. Murray and M. Epstein, April 1976.

56. *An Elastic Stress Analysis of a Gentilly Type Containment Structure - Volume 2 - (Appendices B to F)* by D.W. Murray and M. Epstein, April 1976.

57. *A System of Computer Programs for the Large Deformation In-Plane Analysis of Beams* by M. Epstein and D.W. Murray, May 1976.

58. *A Statistical Study of Variables Affecting the Strength of Reinforced Normal Weight Concrete Members* by S.A. Mirza and J.G. MacGregor, December 1976.

59. *The Destabilizing Forces Caused by Gravity Loads Acting on Initially Out-Of-Plumb Members in Structures* by D. Beaulieu and P.F. Adams, February 1977.

60. *The Second-Order Analysis and Design of Reinforced Concrete Frames* by G.S. Mathews and J.G. MacGregor, January 1977.

61. *The Effects of Joint Eccentricity in Open Web Steel Joists* by R.A. Matiisen, S.H. Simmonds and D.W. Murray, June 1977.

62. *Behaviour of Open Web Steel Joists* by R.A. Kaliandasani, S.H. Simmonds and D.W. Murray, July 1977.

63. *A Classical Flexibility Analysis for Gentilly Type Containment Structures* by D.W. Murray, A.M. Rohardt, and S.H. Simmonds, June 1977.

64. *Substructure Analysis of Plane Frames* by A.A. Elwi and D.W. Murray, June 1977.

65. *Strength and Behavior of Cold-Formed HSS Columns* by Reidar Bjorhovde, December 1977.

66. *Some Elementary Mechanics of Explosive and Brittle Failure Modes in Prestressed Containments* by D.W. Murray, June 1978.

67. *Inelastic Analysis of Prestressed Concrete Secondary Containments* by D.W. Murray, L. Chitnuyanondh, C. Wong and K.Y. Rijub-Agha, July 1978.

68. *Strength of Variability of Bonded Prestressed Concrete Beams* by D.K. Kikuchi, S.A. Mirza and J.G. MacGregor, August 1978.

69. *Numerical Analysis of General Shells of Revolution Subjected to Arbitrary Loading* by A.M. Shazly, S.H. Simmonds and D.W. Murray, September 1978.

70. *Concrete Masonry Walls* by M. Hatzinikolas, J. Longworth and J. Warwaruk, September 1978.

71. *Experimental Data for Concrete Masonry Walls* by M. Hatzinikolas, J. Longworth and J. Warwaruk, September 1978.

72. *Fatigue Behaviour of Steel Beams with Welded Details* by G.R. Bardell and G.L. Kulak, September 1978.

73. *Double Angle Beam-Column Connections* by R.M. Lasby and Reidar Bjorhovde, April 1979.

74. *An Effective Uniaxial Tensile Stress-Strain Relationship for Prestressed Concrete* by L. Chitnuyanondh, S. Rizkalla, D.W. Murray and J.G. MacGregor, February 1979.

University of Alberta

Department of Civil Engineering

An Effective Uniaxial Tensile Stress-Strain Relationship for Prestressed Concrete

by

L. Chitnuyanondh

S. Rizkalla

D.W. Murray

and

J.G. MacGregor

A Technical Report

to

The Atomic Energy Control Board
Nuclear Plant Licencing Directorate
P.O. Box 1046
Ottawa, Canada, K1P 5S9

February 1979

Acknowledgements

The authors wish to acknowledge the cooperation of the following agencies which provided technical information and/or financial support for the overall study.

The Atomic Energy Control Board of Canada
Atomic Energy of Canada, Limited
Hydro-Québec
Canatom Limited
Ontario Hydro

Disclaimer

The interpretation of the technical data and any opinions or conclusions arising in this report are those of the authors only and do not necessarily reflect those of the cooperating agencies.

Abstract

This report evaluates the direct tensile strength and an equivalent uniaxial tensile stress-strain relationship for prestressed concrete using data from specimens tested at the University of Alberta which represent segments from the wall of a containment vessel. The stress-strain relationship, when used in conjunction with the BOSOR5 program [4], enables prediction of the response of prestressed concrete under any biaxial combination of compressive and/or tensile stresses.

Comparisons between the experimental and analytical (BOSOR5) load-strain response of the wall segments are also presented. It is concluded that the BOSOR5 program is able to predict satisfactorily the response of the wall segments and multi-layered shell structures.

TABLE OF CONTENTS

		Page
Title Page		i
Acknowledgements		ii
Disclaimer		ii
Abstract		iii
Table of Contents		iv
List of Tables		vi
List of Figures		vii
Notation		viii
1.	INTRODUCTION	1
	1.1 Background to Report	1
	1.2 Objective of Report	1
	1.3 Structure of Report	3
2.	DERIVATION OF THE UNIAXIAL TENSILE STRESS-STRAIN CURVE FOR CONCRETE	4
	2.1 Literature Review	4
	2.2 Derivation of an Effective Tensile Uniaxial Stress-Strain Curve	7
	2.2.1 General Concepts	7
	2.2.2 Derivation of Effective Tensile Uniaxial Curve from Uniaxially Loaded Specimens	9
	2.2.3 Derivation of Effective Tensile Uniaxial Curve from Biaxially Loaded Specimens	10
3.	PROPOSED STRESS-STRAIN CURVES AND TEST RESULTS	15
	3.1 General	15
	3.2 Cracking Loads of Wall Segments	16
	3.3 Tensile Strengths of Concrete of Wall Segments	17

Page

3.4 Derived Stress-Strain Curves 26

3.4.1 Initial Approximate Stress-Strain Curves for Concrete 26
3.4.2 Tensile Stress-Strain Curves Derived from Test Results 26
3.4.3 Proposed Stress-Strain Curves for Concrete 29
3.4.4 Discussion of the Proposed Tensile Stress-Strain Curve 31

4. COMPARISON OF TEST SEGMENT AND BOSOR5 RESULTS 32

4.1 General 32

4.2 Segment Properties and Modelling 32

4.3 Results of Non-Prestressed Segments 34

4.4 Results of Prestressed Segments 37

4.4.1 Uniaxially Loaded Segments 37
4.4.2 Biaxially Loaded Segments 38

4.5 Effects of the Shape of the Tensile Stress-Strain Curve on BOSOR5 Execution 40

5. CONCLUSIONS 42

REFERENCES 43

TABLES 45

FIGURES 55

APPENDIX A - Consistent Derivation of Uniaxial Tensile Stress-Strain Curve 75

APPENDIX B - Example of the Determination of Cracking Load and Tensile Strength of Concrete 80

LIST OF TABLES

Table	Title	Page
3.1	Properties of Wall Segments	46
3.2	Observed Cracking Loads in Wall Segments	47
3.3	Measured and Computed Strengths of Concrete of Wall Segments	48
3.4	Derived Tensile Strengths for Various Types of Applications	49
4.1	Tensile Stress-Strain Curves used for BOSOR5 Analysis	50
4.2	Compressive Stress-Strain Curves used for BOSOR5 Analysis	53
4.3	Comparison of BOSOR5 Execution Time using Different Tensile Stress-Strain for Concrete	54

LIST OF FIGURES

Figure	Title	Page
2.1	Typical Load-Strain Response of Prestressed Concrete	56
2.2	Equivalent Uniaxial Stress-Strain Relationship for Concrete	57
3.1	Relationship between the Computed Tensile Strengths and Cylinder Strengths	58
3.2	Effect of Biaxial Stresses on Strength at Cracking	59
3.3	Uniaxial Tensile Stress-Strain Curves for Prestressed Concrete	60
3.4	Uniaxial Tensile Stress-Strain Curves for Non-Prestressed Concrete	61
3.5	Typical Load-Strain Response of Segment 5	62
3.6	Stress-Path of Segment 3	63
3.7	Proposed Compressive Stress-Strain Curve for Concrete	64
3.8	Proposed Tensile Stress-Strain Curve for Concrete	64
3.9	Sample Comparison between Analytical and Experimental Tensile Stress-Strain Curves for Concrete	65
4.1	Wall Segment Dimensions	66
4.2	Typical Section A-A through Wall Segment	67
4.3	Typical Section B-B through Wall Segment	67
4.4	Steel Properties for Segment Test	68
4.5	Load-Strain Response of Segment 4	69
4.6	Load-Strain Response of Segment 7	69
4.7	Load-Strain Response of Segment 5	70
4.8	Load-Strain Response of Segment 6	71
4.9	Load-Strain Response of Segment 3	72
4.10	Load-Strain Response of Segment 1	73
4.11	Load-Strain Response of Segment 8	74

Notation

Special Symbols

{ } = a column vector

< > = a row vector

Superscripts and Subscripts

1,2 = subscripts indicating orthogonal directions or a sequence of points.

c = subscript indicating "compression" or "concrete"

e = subscript indicating "effective"

p = subscript indicating "prestress"

s = subscript indicating "steel"

E = superscript indicating "elastic"

P = superscript indicating "plastic"

Roman Letter Symbols

A_c = net area of concrete

A_p = area of prestressing steel

A_s = area of mild steel

A_t = total transformed area

e = eccentricity of the applied load

E_c = initial elastic modulus of concrete

E_p = initial elastic modulus of prestressing steel

E_s = initial elastic modulus of mild steel

f = stress

f'_c = 28 day compressive strength of 6 x 12 cylinder

f''_c = maximum compressive stress of concrete

f_{pe} = effective tensile stress in the prestressing strand after all losses have occurred

f_{pc} = compressive stress in the concrete, after all prestress losses have occurred

f'_t = tensile strength by Brazilian splitting test

f''_t = maximum tensile strength in segment considering bending effects

f_{to} = maximum tensile strength in segment ignoring bending effects

f_{tR} = concrete strength in tension at the loading rate of R psi/sec.

P = total axial load on segment

P_{cr} = load at which first cracking occurs in the concrete

P_c = effective load carried by concrete

P_p = effective load carried by prestressing steel

P_s = effective load carried by mild steel

R = loading rate (psi/sec.)

V = concrete volume in Eq. 2.3

V_0 = concrete volume of a 4 inch cube

X = concrete strength in Eq. 2.3

X_0 = concrete strength of a 4 inch cube

X,Y,Z = a sequence of stress points

Z = section modulus of total transformed area

Greek Letter Symbols

α = fraction of f'_t to determine the effective value for f''_t

ε = strain

$\{\varepsilon\}, \varepsilon_1, \varepsilon_2$ = the vector of total principal strains and its components

$\{\varepsilon^E\}$ = the vector of elastic principal strains

$\{\varepsilon^P\}$ = the vector of plastic principal strains

ε_0 = uniaxial strain corresponding to the maximum compressive stress, f''_c

ε_{pe} = strain in the prestressing steel caused by the effective prestress

ε_{si} = initial prestrain in the concrete and mild steel

ε_u = ultimate compressive strain of concrete

$\bar{\varepsilon}$ = equivalent uniaxial strain

ν = elastic Poisson's ratio

$\{\sigma\}, \sigma_1, \sigma_2$ = the vector of principal stresses and its components

$\bar{\sigma}$ = equivalent uniaxial stress

1. INTRODUCTION

1.1 Background to Report

This report is a sequel to the report entitled "Inelastic Analysis of Prestressed Concrete Secondary Containments", [14], which dealt with the development of analytical capabilities for the prediction of nonlinear response of nuclear containment structures. This analytical study relied extensively on the data from tests of reinforced and prestressed concrete "wall segments" representing portions of the wall of a containment vessel. These tests were carried out under a parallel experimental program at the University of Alberta with the primary objective that comparisons could be made between analytical and experimental results. Figures 4.1 to 4.3 discussed later in this report, show the overall layout of these specimens. At the time Ref. 14 was written, nine of fourteen wall segments had been tested, but the data was not fully processed. Based on the results of the first three wall segment tests, it was shown in Ref. 14 that a proposed elastic-plastic constitutive model for concrete, when used with the BOSOR5 program [4], was adequate for a simulation of experimental results.

During the period between the writing of Ref. 14 and the present, the remaining data has been processed. This allows further conclusions to be drawn in connection with the nonlinear tensile behavior of concrete, as presented in this report.

1.2 Objective of Report

A fundamental requirement of analysis with the proposed elastic-plastic constitutive model for concrete [14] is an adequate characterization

of the concrete behavior, which forms a part of the input of the structure to be analyzed with the BOSOR5 program. The concrete behavior is characterized, in the constitutive model, by two individual uniaxial stress-strain curves, one for tension and one for compression. These input curves remain unchanged throughout the loading history of the structure irrespective of any change in the state of the biaxial stress of the concrete. The constitutive model determines which point on the stress-strain curve is pertinent to each of the two principal stress directions. Such a point provides the basic properties of the concrete, such as the hardening parameter and the stiffness of the concrete, for a given equivalent plastic strain.

The uniaxial stress-strain curves were initially estimated from published results of uniaxial tests on plain concrete prisms, as described in Ref. 14. (Sects. 2.5.3 and 2.5.4).

A certain amount of engineering judgement was involved in the estimation. An attempt is made, therefore, in this report to obtain more reliable estimates of the tensile stress-strain curve using the experimental data from a wider spectrum of the test segments. Briefly, the primary objectives are:

1. To rationally derive a tensile stress-strain curve for concrete for use with the elastic-plastic constitutive model of Ref. 14.
2. To obtain an estimate of the strength of concrete in direct tension, as it is exhibited in reinforced and prestressed wall segments.
3. To make additional comparisons between the predicted analytical and the experimental response of the test segments. This serves as a

verification of the uniaxial stress-strain curves, as derived herein, and of the analytical technique.

1.3 Structure of Report

A short literature review of experimental and theoretical stress-strain curves for concrete is presented in Sect. 2.1. The formulation required to derive a tensile stress-strain curve for concrete, based on the test segment data, is contained in Sect. 2.2.

Sections 3.2 and 3.3 discuss the observed cracking loads of the wall segments and compute the tensile strength of the concrete in each of the segments. The factors that may affect the tensile strength are also discussed.

Based on the measured strains of the test segments, the tensile stress-strain curve for concrete is computed for each of the test segments in the remaining part of Chapter 3. A lower bound for the degrading branch is then proposed.

Comparisons between the analytical and experimental load-strain response of the test segments is made in Chapter 4. Conclusions are contained in Chapter 5.

2. DERIVATION OF THE UNIAXIAL TENSILE STRESS-STRAIN CURVE FOR CONCRETE

2.1 Literature Review

Since the present test program deals with specimens tested in tension rather than compression, the uniaxial stress-strain curve in compression is relatively unimportant. Therefore, only a scanty literature review is provided on this aspect of concrete behavior.

Extensive surveys of experimental and theoretical stress-strain curves in uniaxial compression have been carried out by Sargin [18] and by Popovics [17]. Sargin pointed out that there are numerous factors that could affect the response of concrete to external loads such as the strength of the concrete, lateral reinforcement, time, strain gradient and specimen size. He, therefore, proposed a theoretical stress-strain relationship for concrete under flexural compression which accounts for the above factors. The form of the relationship is, as expected, quite complicated.

To date, one of the most widely used theoretical stress-strain curves is that proposed by Hognestad [7] in 1951. Although the relationship does not reflect all the factors mentioned above, it at least accounts for the variation of the initial elastic modulus, E_c, and the compressive strain, ε_o, corresponding to the maximum stress, f''_c, as the compressive strength of the control cylinder, f'_c, varies. The relation is of the form:

$$f_c = f''_c \left[2\varepsilon/\varepsilon_o - (\varepsilon/\varepsilon_o)^2\right] \qquad \text{for } \varepsilon \leq \varepsilon_o \qquad (2.1a)$$

$$f_c = f''_c (\varepsilon_u - 0.85\ \varepsilon_o - 0.15\varepsilon)/(\varepsilon_u - \varepsilon_o) \qquad (2.1b)$$

$$\text{for } \varepsilon > \varepsilon_o$$

where ε_u is the ultimate strain, which is assigned a constant value of 0.0038. f''_c assumes a constant relationship to f'_c ($= 0.85\ f'_c$), and E_c is given by

$$E_c = 18{,}000 + 0.46\ f'_c \qquad (2.2)$$

Equation 2.1 has proven to be adequate on many investigations and is adopted herein.

Theoretical simulation of the tensile stress-strain curve is, unfortunately, much more difficult since experimental investigation is sparse. To obtain the complete experimental stress-strain response, the testing machine must be rigid and the loading platen properly designed. By making sure these requirements were satisfied Evans and Marathe [6], and Hughes and Chapman [8] were able to successfully obtain complete curves using plain concrete prismatic specimens loaded uniaxially. The curves show a degrading stiffness similar to that of the compression curve. Ref. 6 indicates that the peak tensile strength may occur at strains between 0.00015 and 0.0008 and that the secant modulus of elasticity drops rapidly on the falling branch of the stress-strain curve, reaching an average value of 0.25×10^6 psi at a strain of about 0.0006 compared to an initial tangent modulus of roughly 12 times that amount. Nevertheless, the specimens were able to attain a strain well above 0.001 before failure occurred and the corresponding stresses varied between 25 to 40 percent of the maximum tensile strength. Microcracking occurred at strains between 0.00009 and 0.00014.

A detailed documentation of the factors that affect the cracking and ultimate tensile strengths of concrete is given by Neville [15]. Variation of tensile strengths between similar test cylinders can be caused by loading rate and the moisture condition during testing. A further variation in the tensile strengths is expected between the concrete in the test cylinder and a structural test specimen. The more important factors are differences in the curing conditions, size effects, the effect of reinforcement on the mode of cracking in the specimen, and the different stress regimes in the cylinder and specimen at cracking. The mode of cracking, (i.e. - flexural tensile cracking or direct tensile cracking, or cracking in a biaxial compression-tension field as in a split cylinder test), influences the cracking strength that the concrete can develop. Neville [15] reported that a size effect is reflected in the ratio of the smallest dimension of the test specimen to the maximum aggregate size. The higher the ratio, the less pronounced is this size effect.

Several investigators have used the weakest link theory to relate the tensile strength of concrete to the volume of concrete under high stress. Linder and Sprague [10] reported a 15 percent decrease in the modulus of rupture between 6 and 18 inch deep beams and explained this using such a theory. Malhotra [11] reported that the tensile strength of a 4 in. diameter cylinder is greater than that of a 6 in. diameter cylinder. Typically the difference would be about 13 percent for cylinders with a nominal strength of 400 psi. Bolotin [3] has presented Eq. 2.3 to relate the strength, X, of a given specimen of volume V to that of a 4 in. cube stressed in direct tension and having a strength and volume of X_o and V_o.

$$X = X_o \left\{0.43 + 0.57 \left(\frac{V_o}{V}\right)^{1/3}\right\} \qquad (2.3)$$

As V goes to infinity, X approaches 0.43 X_o.

A further factor affecting cracking in reinforced concrete structures is the presence of reinforcement. Such aspects as bar cover, bar spacing, transverse reinforcing, percentage of reinforcement, and multiaxial stress conditions may all be expected to have an influence on the cracking behavior and the tensile strength of concrete.

2.2 Derivation of an Effective Tensile Uniaxial Stress-Strain Curve

2.2.1 General Concepts

One of the main objectives of the experimental test program at the University of Alberta is to provide data for the derivation of an effective uniaxial tensile stress-strain curve for concrete, which is adequate to allow a reliable simulation of the response of wall segments subjected to tensile membrane forces. The test specimens included both non-prestressed and prestressed wall segments subjected to either uniaxial or biaxial tensile forces.

For a specimen in tension, the internal force distribution between the concrete and the steel before cracking occurs is a function of the material stiffnesses. After cracking, the concrete stress drops to zero at the crack, as shown by the simple example in Sect. 2.1 of Ref. 14. However, bond stress is developed between the concrete and steel which prevents the effective stress in the concrete from reducing to zero along the entire length of the specimen. The entire load would be carried by the steel at the location of a 'through-crack', but the strain associated with the maximum steel stress occurs only over a short length of the steel. The average

strain in the specimen is considerably less than the maximum steel strain and provides a means of determining the average internal force to be attributed to the concrete in order to simulate the proper wall stiffness of the section. The average strain is easily measured in a tensile test.

Redistribution of forces during the progressive deterioration of a structure is dependent on the relative overall stiffnesses of the components and not upon the maximum stresses at specific points. Average crack widths and distributions are also dependent on overall stiffnesses rather than stresses at specific points. Therefore, to reliably predict redistribution, cracking, and consequently leakage, in a complex structure it is necessary to predict average strains in concrete subjected to tensile effects. The concept of retaining a residual stress in the concrete is necessary if accurate predictions of strains and deformations are to be made for membrane tension states in prestressed concrete wall segments. The effective stiffness of the concrete is reduced, of course, as more and more cracks form and ultimately the stiffening effect of the concrete disappears as the stress becomes almost totally transferred to the steel. Since the degrading part of the derived stress-strain curve is a function of the average strain, which in turn is dependent on the crack width and distribution, its shape may be expected to vary. Crack widths and distribution are themselves dependent on numerous factors such as the concrete cover, reinforcement ratio, bar size and yield strength of the reinforcement. By necessity, the current experimental test program is very limited and does not allow any extensive investigation of the effects of these parameters on the degrading part of the stress-strain curve.

The equivalent uniaxial stress-strain curve can be derived from either the uniaxially or biaxially loaded specimens. If it is true that biaxial tensile response can be related to uniaxial tensile response, and if the proper form of this relationship is known, the effective uniaxial curves deduced from either type of specimen should be similar. The techniques used herein of attempting to deduce such a uniaxial curve from each of these types of specimens are discussed below.

2.2.2 Derivation of Effective Tensile Uniaxial Curve from Uniaxially Loaded Specimens

The load-strain response of the mild steel and the concrete in a prestressed wall segment are schematically shown as the left-hand curve in Fig. 2.1. The average measured strain, ε, in the direction of the applied load, P, is recorded only when the load is applied and is zero when the load is zero. However, strains already exist in the wall segment due to the prestressing operation. The prestressing operation induces a tensile strain, ε_{pe}, in the prestressing steel and a small compressive strain, ε_{si}, in the mild steel and concrete. It is assumed that ε_{pe} is the effective strain in the prestressing steel after all creep, relaxation and shrinkage losses, and that f_{pe} is the associated stress. It is simple to compute the total strain in the prestressing steel at any stage of the loading from test observations if ε_{pe} is known. Because of compatibility in a bonded prestressed specimen, the difference between the strains in the mild steel and prestressing steel should remain constant and equal to $|\varepsilon_{si}| + \varepsilon_{pe}$, as shown in Fig. 2.16, during any short term loading. Then neglecting redistribution due to creep,

$$\varepsilon_{pe} = f_{pe}/E_p \tag{2.4}$$

$$\varepsilon_{si} = - f_{pe} A_p/E_c \quad (A_c + E_s A_s/E_c) \tag{2.5}$$

where E_p, E_s and E_c are the short term modulii of elasticity of the prestressing steel, mild steel and concrete, respectively, A_p is the area of the prestressing steel, A_s is the area of the mild steel, and A_c is the net area of the concrete.

At any given load P, the force carried by the concrete, P_c, is

$$P_c = P - P_s - P_p \tag{2.6}$$

where P_s and P_p are the forces carried by the mild steel and prestressing steel, respectively. P_s and P_p can be calculated from the average measured strain and hence Eq. 2.6 becomes,

$$P_c = P - E_s A_s (\varepsilon + \varepsilon_{si}) - E_p A_p (\varepsilon + \varepsilon_{pe}) \tag{2.7}$$

in which ε is the observed or measured strain.

Eq. 2.7 leads to the effective stress in the concrete being,

$$\sigma_c = P_c/A_c \tag{2.8}$$

The equivalent uniaxial stress-strain curve is obtained by plotting σ_c vs ε.

2.2.3 Derivation of Effective Tensile Uniaxial Curve from Biaxially Loaded Specimens

The derivation of an effective uniaxial stress-strain curve, consistent with the constitutive model of Ref. 14 , from a biaxially loaded wall segment involves a definition of a yield curve in biaxial stress space and a procedure of calculating the plastic strains. Consider a wall segment being loaded biaxially with a constant load ratio, creating a concrete stress ratio which, due to the degrading nature of concrete, is not constant. The stresses in the concrete at

three load steps are plotted as points Z, Y, X in biaxial stress space, as shown in Fig. 2.2a. If the shape of the yield curve for concrete in the biaxial stress space is known, then the yield stresses corresponding to the three stress points may be represented by $(\bar{\sigma}_{Z1}, \bar{\sigma}_{Z2})$, $(\bar{\sigma}_{Y1}, \bar{\sigma}_{Y2})$ and $(\bar{\sigma}_{X1}, \bar{\sigma}_{X2})$ in Fig. 2.2a. These stresses are the equivalent uniaxial yield stresses. It is to be noted that there can be many combinations of yield stresses for each yield curve if the chosen yield curve is non-symmetrical. Appendix A describes a technique by which the yield stresses may be determined in a manner completely consistent with the yield theory, providing sufficient experimental points are available.

However, since only one of the values of the yield stresses is required to plot a curve, we will use a simple approach and select the one that corresponds to the direction that cracks and softens first. Although this procedure is not strictly defensible, the scatter of the test results is such that the more sophisticated treatment of appendix A does not appear warranted. The choice of a function for the yield curve should rely on experimental results, such as those of Kupfer, Hilsdorf and Rüsch [9]. Various suitable functional forms have been discussed in Sect. 2.4 of Ref. 14. In its simplest form the yield curve in the tension-tension zone approaches a rectangle, implying that the yield stresses in the two principal directions are independent of each other. For the derivation of the stress-strain curve, herein, a rectangular yield curve is assumed, as shown in Fig. 2.2c, because of its simple form.

For each of the stress points, say at point X in Fig. 2.2a, the equivalent uniaxial strain is given by (see Fig. 2.2b)

$$\bar{\varepsilon}_X = \bar{\varepsilon}_X^P + \bar{\varepsilon}_X^E \tag{2.9a}$$

or

$$\bar{\varepsilon}_X = \bar{\varepsilon}_X^P + \frac{\bar{\sigma}_X}{E_c} \tag{2.9b}$$

where $\bar{\varepsilon}_X^P$ is the equivalent uniaxial plastic strain, $\bar{\sigma}_X$ is the yield stress consistent with this level of yield curve and $\bar{\varepsilon}_X$ is the equivalent uniaxial total strain.

In order to compute the unknowns, $\bar{\varepsilon}_X^P$ and $\bar{\sigma}_X$, the stresses in the concrete in the two loaded directions are first obtained in the concrete in the same manner as in the uniaxially loaded case. The forces carried by the concrete are,

$$P_{c1} = P_1 - E_s A_{s1}(\varepsilon_1 + \varepsilon_{si,1}) - E_p A_{p1}(\varepsilon_1 + \varepsilon_{pe,1}) \tag{2.10a}$$

$$P_{c2} = P_2 - E_s A_{s2}(\varepsilon_2 + \varepsilon_{si,2}) - E_p A_{p1}(\varepsilon_2 + \varepsilon_{pe,2}) \tag{2.10b}$$

where the subscripts 1 and 2 denote the direction. It should be noted that no Poisson's ratio correction is needed for ε_1 and ε_2 in the above equations because the steel bars behave uniaxially. The concrete stresses are,

$$\sigma_{c1} = P_{c1}/A_{c1} \tag{2.11a}$$

$$\sigma_{c2} = P_{c2}/A_{c2} \tag{2.11b}$$

Having chosen the rectangular yield curve of Fig. 2.2c, the yield stress corresponding to the stress point $(\sigma_{c1}, \sigma_{c2})$ is $\bar{\sigma}_2 = \sigma_{c2}$, while $\bar{\sigma}_1$ is not defined, as shown in Fig. 2.2c. Therefore, the required single yield stress $\bar{\sigma}$ is obtained as

$$\bar{\sigma} = \bar{\sigma}_1 \quad \text{if direction 1 cracks first}$$

$$= \bar{\sigma}_2 \quad \text{if direction 2 cracks first (as in the illustration of Fig. 2.2)} \tag{2.12}$$

The elastic strains in the concrete are

$$\varepsilon_1^E = (\sigma_{c1} - \nu\sigma_{c2})/E_c \tag{2.13a}$$

$$\varepsilon_2^E = (\sigma_{c2} - \nu\sigma_{c1})/E_c \tag{2.13b}$$

where ν is the Poisson ratio, and the plastic strains are

$$\varepsilon_1^P = \varepsilon_1 - \varepsilon_1^E \tag{2.14a}$$

$$\varepsilon_2^P = \varepsilon_2 - \varepsilon_2^E \tag{2.14b}$$

The above plastic strain vector, $< \varepsilon^P >$, can be converted into a total equivalent plastic strain $\bar{\varepsilon}^P$, in the normal manner, as

$$\bar{\varepsilon}^P = \sqrt{< \varepsilon^P > \{ \varepsilon^P \}} \tag{2.15}$$

Hence, the total equivalent uniaxial strain is computed from Eq. 2.9b and is

$$\bar{\varepsilon} = \bar{\varepsilon}^P + \frac{\bar{\sigma}}{E_c} \tag{2.16}$$

Thus, knowing the section properties of the wall segment, the measured values P_1, P_2, ε_1, ε_2 and the initial values $\varepsilon_{si,1}$, $\varepsilon_{si,2}$, $\varepsilon_{pe,1}$, $\varepsilon_{pe,2}$, the equivalent uniaxial stress $\bar{\sigma}$ and the equivalent uniaxial strain $\bar{\varepsilon}$ can be calculated.

The determination of the uniaxial stress-strain curves from biaxial test results, as presented subsequently herein, has been carried out according to Eqs. 2.10 to 2.16.

3. PROPOSED STRESS-STRAIN CURVES AND TEST RESULTS

3.1 General

Uniaxial stress-strain curves for concrete are proposed in this chapter. The compression curve is simply a modified form of the curve first proposed by Hognestad [7]. The appropriateness of such a choice is of no great importance in the present investigation because failure in the test structure, and other secondary containments, is expected to be by tensile failure of the reinforcement prior to any significant crushing of concrete. Hognestad's curve [7] has proved to be adequate up to the maximum stress, based on a statistical analysis carried out by Mirza, Hatzinikolas and MacGregor [13], and has been sufficiently reliable to be used in many other studies.

The final proposed tensile stress-strain curve is determined from the measured strains of the wall segments, using the equations derived in Sect. 2.2. In Ref. 14, two approximate tensile stress-strain curves for concrete were initially adopted, using published results for plain concrete as a guide. Those curves were obtained in a rather arbitrary manner, relying on a certain amount of engineering judgement, but gave good results in BOSOR5 simulations of Specimens 1 and 3. The final form recommended in this report is similar to the revised curve of Fig. 4.28 of Ref. 14. Thus the effect of this report is to confirm the suitability of the revised form tentatively proposed in Ref. 14.

Comparisons between the analytical and experimental response of the additional wall segments are also given in the present report. The basic properties of the wall segments are given in Table 3.1, where they are grouped according to the type of prestressing and loading. The specimens cover a range of details including variations in concrete cover, bar size, and percentage reinforcing. Only 8 of the 14 specimens have been considered in this study. The remaining 6 specimens were tested to investigate special problems such as splices, leakage and applied moments.

There are two primary effects which can be determined from the test results:

(a) the effective tensile strength of the concrete as evidenced by cracking of the concrete in the presence of the details inherent in the specimen, and

(b) the effective stress-strain response of the segments in the post-cracking response range.

Neither of these effects would be expected to be completely independent of the aforementioned details. Therefore, considerable scatter in results may be expected.

The problem of determining the 'cracking strength' or tensile strength is addressed in Sects. 3.2 and 3.3. The problem of determining a representative effective tensile stress-strain curve is addressed in Sect. 3.4.

3.2 Cracking Loads of Wall Segments

The cracking load of each segment needs to be accurately determined in order to compute the effective tensile strength of the concrete.

Cracking loads are tabulated in Table 3.2. The cracking load is taken to be the first change of the slope of the load-strain relationship taking into account the visual observation of crack initiation during the tests and the load at which cracks crossed surface mounted strain gages. The assessment is complicated by the unavoidable presence of small bending moments in the wall segments, although the loads were intended to be applied concentrically. This bending caused the concrete on each face of a segment to crack at different loads. For example, the load-strain relationships for each face of Specimen 9 indicate that the cracking load of face A can be taken as 350.0 kips whereas that of face B is only 300.0 kips (Table 3.2). Thus, the lower value is assumed to be the true cracking load. Such inspection was carried out for each of the loaded directions for a biaxially loaded specimen. The underlined values in Table 3.2 are the ones from which the tensile strengths of concrete are computed. Under the column heading of 'overall cracking load' in Table 3.2, the cracking loads obtained from the average load-strain relationships are given: that is, the effectof bending is ignored.

Appendix B outlines the technique of arriving at the cracking loads in Table 3.2, using Specimen 1 as an example.

3.3 Tensile Strengths of Concrete of Wall Segments

The 'true' tensile strength f''_t, of the concrete in each of the wall segments is calculated from the following equation

$$f''_t = \frac{P_{cr}}{A_t} + \frac{P_{cr}e}{Z} - f_{pc} \qquad (3.1)$$

where P_{cr} is the cracking load, e is the eccentricity of the applied load and is calculated from the strain gradient across the thickness of the wall segment, Z is the section modulus and f_{pc} is the compressive stress in the concrete after all prestress losses have occurred. A value of f''_t is computed from each of the loaded directions using the appropriate values of P_{cr} from Table 3.2 and the lower value is taken as the tensile strength for that specimen.

Eq. 3.1 indicates that the f''_t value is highly dependent on f_{pc}, which is computed from the effective prestress at the start of the test. The prestress losses from the time of the jacking operation to the time of grouting were measured with load cells on the tendons. Once the grout had hardened the load cells could not be used and subsequent losses were computed by an analytical procedure. The details of this computation will be presented in subsequent reports on the experimental phase. In the derivations presented in this report, lump sum losses of 12 percent were assumed in the vertical direction where four, seven-wire tendons had a nominal initial prestress of 153 ksi and 8 percent in the horizontal direction where three, six-wire tendons had a nominal initial prestress of 135 ksi. These values were representative of the sum of the measured and computed losses in all specimens.

The computed tensile strengths are shown in Table 3.3. Column 7 gives values computed with the applied moments taken into account, whereas column 8 gives the tensile strengths when the moments are excluded. As expected, the former values are higher than the latter values, and those values (column 7) have been taken as the 'true' tensile strengths of the concrete. Appendix B illustrates the computations involved in determining these values for Specimen 1.

Before going on to discuss the individual values it is important to note the relative accuracy of the computed tensile strengths. The example computations in Appendix B show that the possible errors in the measurement of the loads, prestress and areas are such that there is a 95 percent probability that the computed tensile strength is within ± 11 percent of the actual tensile stress at cracking for Specimen 1.

The computed tensile strengths are compared in Fig. 3.1 and Table 3.3 to the splitting tensile strengths of the corresponding cylinders and to the square root of f'_c. The scatter is large in both cases. It can be attributed to the combination of scatter in the relationship between tensile and compressive strength of concrete, and the possible errors in computing the stresses at cracking of the specimens. The mean tensile strength measured in the specimen tests, as computed from columns 9 and 10 of Table 3.3, is 0.6 times the splitting tensile strength or 3.65 $\sqrt{f'_c}$. The best fit relationship to the data is indicated in Fig. 3.1b by the dashed line, which suggests that f''_t is related to some power of concrete strength between 1/2 and 1.

The tensile stress at cracking is considerably lower than that generally accepted in structural design. Thus, the 1977 ACI Code bases the calculation of the flexural cracking load that governs shear strength in Section 11.4.2.1 on $6\sqrt{f'_c}$. Similarly, the extreme fiber stress in tension in precompressed tension zones is allowed to reach $6\sqrt{f'_c}$ under service loads (Section 18.4.2(b)).

Several reasons may be advanced for this apparently low cracking strength. These effects are examined in detail as follows.

(a) Aggregate Size Effects

When the size of the aggregate is large compared to the size of the specimen the tensile strength relationships are affected. This was not the case, however, in either the wall segment specimens or the test cylinders, and the aggregate size effect cannot be considered as contributing to the observed strength reduction.

(b) Specimen Size Effects

Several studies of the effect of specimen size on tensile strength were reported in Chapter 2. None of these specifically dealt with the problem of conversion from a splitting test to a direct tension test. If, however, it is assumed on the basis of photo-elastic tests of discs loaded across a diameter that the volume subjected to maximum tensile stress in a splitting test of a 6 x 12 cylinder extends over the middle 80 percent of the loaded diameter and 1 inch each way from the diameter, the effective volume of such a specimen would be roughly 115 in^3. Applying Eq. 2.3 suggests that a wall segment specimen with a volume of 10400 in^3 should have a tensile strength of 60 percent of that of a split cylinder test. This assumes the specimen is in pure tension, but due to accidental moments this was not true. If the volume reduction were arbitrarily based on the volume of the outer inch of the wall segment the tensile strength obtained from Eqn. 2.3 would be 68 percent of the split cylinder strength. Thus, the 60 percent value measured is probably in part due to the volume effect.

(c) Prior Shrinkage Cracks

All the segments had surface shrinkage cracks on the face which was exposed to the air when the specimen was cast, and in some

cases the first tensile cracks initiated from these cracks. No trend is discernable in the data concerning the effect of these cracks on the load at which cracking occurred in the tests. Thus, for example, the first crack due to loading appeared on the precracked surface in 4 of the 9 specimens.

(d) Ratio of Applied Stresses

Experimental results in Ref. 9 indicate that the tensile strength of concrete under biaxial tension is almost independent of the stress ratio at the time of cracking and is equal to the uniaxial tensile strength. In the tests reported here, the average ratios of f''_t/f'_t were 0.51, 0.57, and 0.78, respectively, for loading ratios of 1:1, 1:2 and 1:0 in the two directions. The corresponding ratios of $f''_t/\sqrt{f'_c}$ were 3.10, 3.76 and 4.23, respectively. Due to the different prestressing forces in the two directions and the accidental moments due to eccentricity of the loads, the ratio of the stresses at cracking was not the same as the ratio of forces. In Fig. 3.2(a) and (b) the ratio of tensile strength at cracking to either f'_t or $\sqrt{f'_c}$ is plotted vertically while the ratio of the transverse stress at the same load to f'_t or $\sqrt{f'_c}$ is plotted horizontally. Although there is a great deal of scatter it would appear that the strength at a stress ratio of 1:1 is less than that for a stress ratio of 1:0. Lines representing a square interaction diagram in the biaxial tension region are plotted in Fgiures 3.2 and this assumption will be used in the derivation of the tensile stress-strain curves.

(e) Method of Loading

The loads were introduced as concentrated loads applied through the reinforcing bars and tendons, where these extended from the specimen.

In effect, this represented the load transfer across a pre-existing crack. To avoid end effects, the zone in which measurements were made was limited to the middle portion of the specimen. It does not appear that the method of load introduction affected the stresses at cracking at the points where the first cracks developed within these zones.

(f) Stress Concentrations

The presence of transverse bars near the concrete surfaces may have affected the strength in this region, either by causing a stress concentration during the test or by causing more shrinkage micro-cracking adjacent to the bars. The close similarity between the cracking pattern and the bar arrangement suggests there may be some reduction in strength adjacent to transverse bars. It should be noted that crack patterns observed in tests or structures frequently mirror the reinforcement pattern.

(g) Loading Rate

Still another factor that might have lowered the tensile strength of the concrete in the wall segments is the rate of application of the load. Mirza, et al. [13] have suggested that the effect of the rate of loading on flexural and splitting tension strengths of concrete can be described by the following equation:

$$f_{tR} = 0.96\, f_{t2.5}\, (1 + 0.11 \log_{10} R) \qquad (3.2)$$

where $f_{t2.5}$ is the concrete strength in direct tension at the loading rate of 2.5 psi/sec which roughly corresponds to the rate of loading of the control tension cylinders and f_{tR} is the tensile strength to be computed at a loading rate of R psi/sec. As an example, consider

specimen 1 in which the first cracks were observed 1.5 hours from the start of the test. The splitting strength of the concrete was 490 psi and the concrete had a precompression of 676 psi. Therefore, the loading rate was (490 + 676)/(1.5 x 60 x 60) = 0.216 psi/sec. Applying Eq. 3.2 the apparent strength of the wall segment concrete, f_{tR}, is 0.89 times that measured by the control specimens.

(h) Type of Control Specimen

Different types of tensile tests give differing tensile strengths. Thus, for example the European Concrete Committee [5], states that for 28 day old concrete, the mean tensile strength of a 6 in sq. prism, 12 in or more in length loaded in direct tension, is only 86 percent of that obtained from a split cylinder test. At least a part of this difference is due to the greater volume of concrete under high stress. Thus, assuming the effective volume of a split cylinder specimen is 115 in^3, as computed earlier, and taking the volume of a 6 x 12 cylinder used for a direct tension test as 339 in^3, Eq. 2.3 predicts that the direct tensile specimen should have a mean strength of 84 percent of that of a corresponding split cylinder test. It seems therefore, that the differences in strengths for various types of specimens is largely a function of the different volumes involved.

(i) Summary

The tensile stresses upon first cracking of the segments were approximately 0.6 times the split cylinder strengths or $3.65\sqrt{f'_c}$. The primary cause of this reduction in strength is believed to be the fact that a larger volume of concrete is subjected to high tensile stress in a wall segment test than in a split cylinder test. This is coupled

with strength reductions due to the somewhat slower loading rate in the segment tests and the presence of stress concentrations.

In a full scale structure the volume under stress would be very large and, based on Eqn. 2.3, only 48 percent of the tensile strength could be counted on. On the other hand, the loading rate would be somewhat faster than in a test cylinder. Thus, assuming a 10 second rise time to a pressure sufficient to crack the walls in an overload situation and assuming a tensile strength of 400 psi and a prestress of 600 psi, the rate of loading is roughly (400 + 600)/10 = 100 psi/sec. In such a case, Eqn. 3.2 indicates a basic tensile strength of 1.17 times that from a standard lab test. This effect, coupled with the volume reduction leads to an effective tensile strength of 56 percent of the split cylinder strength in a prototype structure. This could also be expressed as $3\sqrt{f'_c}$.

In the test structure at the University of Alberta, the volume under stress is also very large and similarly only 48 percent of the tensile strength would appear to be effective, based on Eq. 2.3. The loading rate would be very slow in the test structure as it would require about 4 hours to crack the walls. Again, assuming a tensile strength of 400 psi and a prestress of 600 psi, the rate of loading is roughly (400 + 600)/(4 x 60 x 60) = 0.069 psi/sec. Applying Eqn. 3.2, the apparent tensile strength due to the slow loading rate would be 0.87 times the standard split cylinder. Coupling the effects of volume and loading rate, the effective tensile strength would be 42 percent of that of the split cylinder. It is believed that the 37

percent is too low. The volume effect, as expressed by Eq. 2.3, was originally derived from results of unreinforced beams having similar shapes, and tested to determine the modulus of rupture. In such a test, the first initiating crack will lead to abrupt failure of the beam. Therefore, the larger the beam is, the greater is the probability of a weak link (flaw) being subjected to the critical stress which leads to ultimate failure. In the case of the test model, a weak link would only cause local micro-cracking which, because of the reinforcement and the restraints offered by the whole structure, would not propagate if the load were held constant. Moreover, such micro-cracks are not likely to be detected either by visual inspection during testing or by examining the measured strains. In applications, then, initial cracking is only significant in so far as it leads to a more generalized cracking throughout the structure. Nevertheless, a volume effect is the most rational theory upon which to base predictions of the cracking phenomenan.

A summary of the volume and rate effects and the effective reduction factor, computed from them, is shown in columns (2) to (4) of Table 3.4. Column (5) of Table 3.4 indicates the α values found most effective in B050R5 simulations for the two types of applications with which the investigators have had the opportunity to correlate with experimental results. In both of these situations, the effective α exceeds that computed on the basis of the theoretical effects described herein. It appears that the theory underestimates the effective tensile strength by about 15%.

3.4 Derived Stress-Strain Curves

3.4.1 Initial Approximate Stress-Strain Curves for Concrete

Two approximate tensile stress-strain curves for concrete were initially derived from published results of plain concrete, as discussed in Ref. 14. The central idea in the approximation is to allow the concrete to degrade after the peak strength is reached. The degradation is such that only a small residual strength in the concrete is retained at the yield of the reinforcement, so that yielding of the reinforcement is properly simulated.

The first approximation was used as input for the BOSOR5 computer analyses of the wall segments and the first models of the test structure [14]. The second approximation has been used for some of the analyses in this report and for one segment run in Ref. 14. Both are shown on Fig. 3.3.

3.4.2 Tensile Stress-strain Curves Derived from Test Results

Tensile stress-strain curves for concrete have been derived from the wall segment tests using the techniques described in Sect. 2.2 and are plotted in Figs. 3.3 and 3.4. For each segment, the strains used in the derivation are averaged from the surface concrete strains (using 5 inch Demec gages) measured on both faces of the segment. Strains only within the central 20 x 20 inch region of the segment are considered so as to eliminate the edge effects due to bond stress and excessive cracking in the load transfer region. The average strains, therefore, reflect the overall response of the concrete on the load deformation diagram with no consideration for the complete loss of stress in the concrete at a crack.

Figure 3.3 contains stress-strain curves for the prestressed segments whereas Fig. 3.4 contains those for the non-prestressed segments. Results for Segment 2 have been excluded from Fig. 3.3 because they do not appear to be consistent with the rest. Each curve has been non-dimensionalized by dividing the computed stress by the computed tensile strength, f_{to}, (see Table 3.2, col. 8) for the corresponding segment. The strength, f_{to}, has been computed without the bending effects on the segment and is chosen because the stresses used in the derived stress-strain curves are calculated without the bending effects. The initial ascending branch of the curves are not available because of insufficient experimental data. The general shape of the curves in Fig. 3.3 clearly indicates that concrete gradually degrades after cracking. It is interesting to note that soon after cracking in Specimen 5 (Curve 5 in Fig. 3.3), the concrete strength picks up and then deteriorates again. This is a rather unusual phenomenon which can also be seen in the load-strain response for this specimen, which is shown in Fig. 3.5. The slopes of the response curve indicate that the segment gained stiffness between the loads of 330 and 375 kips. Although no explanation is offered for the above phenomenon, it coincided with the unloading and reloading of this specimen.

In general, the degradation of the stress-strain curve is not as great as the first approximate stress-strain curve initially adopted in Ref. 14. An exponential regression analysis of the four experimental curves (#1, #3, #5, and #8) of Fig. 3.3 gave Curve A in Fig. 3.3. The slope of the degrading branch resembles the second approximation rather well, although the latter gives a somewhat lower concrete stress for a given strain.

The computed strains corresponding to the peak strengths of the concrete are shown in col. 11 of Table 3.3 . These strains are approximate because the cracking loads were interpolated from the load-strain relationships. The strain varies from 80 x 10^{-6} to 390 x 10^{-6} with a mean value of 220 x 10^{-6}. The fact that the coefficient of variation is 0.55 (Table 3.3, col. 11) means that the scatter is large and that data points are insufficient. Tasuji, et al. [19] found that the magnitude of the tensile strain at cracking was not constant, but markedly increased with the degree of compression in the orthogonal direction. In uniaxial and biaxial tension, they obtained a mean strain of about 150 x 10^{-6} with only slight deviation from the mean. In the present wall segments, the states of stress at the time of cracking vary from biaxial tension-tension to biaxial tension-compression. Therefore, the computed mean strain of 220 x 10^{-6} may have no real meaning. If only the uniaxially loaded segments (Segments 5 and 6) are considered, the mean strain is 165 x 10^{-6} and this correlates well with the value obtained by Tasuji, et al. However, Evans and Marathe [6] have obtained a mean value well over 150 x 10^{-6} whereas Kupfer, et al. [9] have obtained a mean strain of less than 100 x 10^{-6}. Such a variation between the different test series is small considering the difficulties involved in measuring tensile strains. Moreover, variations in the loading rate affect the strain at cracking.

According to Eq. 2.10, the biaxial stresses of the concrete can be computed for any load level using the measured strains. The computed stress history is illustrated for Segment 3 in Fig. 3.6 (line 1). Line 2 represents the results from the BOSOR5 computer run for the same

segment using the first approximation of Fig. 3.3 as input. The two lines agree very well. The important feature that can be seen from the stress path is that as soon as the concrete in direction 2 reaches its maximum tensile strength, as given by points A_1 and A_2 in Fig. 3.6, the direction 2 stress decreases. In the meantime, the stress in direction 1 increases independently of the behavior of the concrete in direction 2, reaching maximum values at B_1 and B_2 at later load levels. The above observation clearly supports the idea of the three-parameter theory for concrete in which the tensile strengths of concrete in any two orthogonal directions are independent of each other.

Segment 3 is a specimen for which the load ratio is 1:1. For segments with a 2:1 load ratio the correspondence between predicted and measured stress histories is not as good.

3.4.3 Proposed Stress-Strain Curves for Concrete

(a) Compressive Stress-Strain Curve

It is proposed that a modified form of the parabolic curve first used by Hognestad [7] be adopted for the compressive curve (Fig. 3.7). This curve is described by the equations.

$$f_c = f''_c \left[2\varepsilon/\varepsilon_o - (\varepsilon/\varepsilon_o)^2\right] \qquad \text{for } \varepsilon < \varepsilon_o \tag{3.3a}$$

$$f_c = f''_c \left(\varepsilon_u - 0.85\,\varepsilon_o - 0.15\varepsilon\right)/(\varepsilon_u - \varepsilon_o) \qquad \text{for } \varepsilon_o < \varepsilon < \varepsilon_u \tag{3.3b}$$

where ε_u is equal to 0.0038, f''_c is the peak stress equal to 0.85 f'_c, ε_o is the strain corresponding to the peak stress and is equal to $2f''_c/E_c$, and E_c is as given by the ACI code [11] as

$$E_c = 57{,}000\sqrt{f'_c} \tag{3.4}$$

The concrete strength f'_c is the only variable considered. The need for a more accurate description of the curve is not required in the type of containment structure under consideration, since failure is primarily of a tensile nature.

(b) Tensile Stress-Strain Curve

The most common analytical form for the tensile stress-strain curve is a straight line from zero stress to the maximum tensile strength beyond which the strength drops to zero (tension cut-off). This simple form is insufficient for any non-linear analysis in which the objective is to obtain a realistic estimate of strain. It is therefore proposed that the ascending branch of the curve be taken as bilinear with the control points shown in Fig. 3.8. The initial tangent modulus of elasticity is the same as for Eq. 3.4. The peak strength f''_t is equal to $\alpha f'_t$ and the strain corresponding to f''_t is 0.00012. For the analysis of the wall segments α should be taken as 0.6, as determined in Sect. 3.3 and verified in Chapter 4.

The descending branch of the curve corresponds to the second approximation shown in Fig. 3.3 which represents an approximate lower bound to the stress-strain curves of the individual biaxially loaded wall

segment tests. Mathematically, this branch has an initial straight portion followed by a curved portion which can be expressed by the exponential relationship

$$f_t = 1.102\, f''_t\, e^{-465\varepsilon} \qquad \text{for } \varepsilon > 0.0003 \qquad (3.10)$$

However, when this stress-strain curve is used as input for the BOSOR5 analysis, it is approximated by linear segments as illustrated in Fig. 3.3.

3.4.4 Discussion of the Proposed Tensile Stress-Strain Curve

A review of past investigations of the tensile stress-strain curve indicates that the shape is dependent on several factors. The ones which were specifically investigated in Ref. 6 were the maximum strength, age and concrete mix. Two typical stress-strain curves from Ref. 6 are plotted in Fig. 3.9 together with the proposed curves. The sets of curves do not coincide but the phenomena being modelled in each case are different. The curves from Ref. 6 represent tests on plain concrete. The reduction in stress occurs due to a reduction in the cross-sectional area and the axial stiffness of the test piece due to cracks extending part way across it. On the other hand, the stress-strain curve derived in this study is an artificial curve used to predict gross strains of reinforced and/or prestressed concrete members which may be cracked completely through. The concept of such a stress-strain curve is described in Section 2.1 of Ref. 14 and Figures 2.1 and 2.2 of that report. Indeed the resemblance between the proposed curves and those from Ref. 6 is only coincidental.

4. COMPARISON OF WALL SEGMENT TESTS AND BOSOR5 RESULTS

4.1 General

The results of the wall segment specimens are compared in this chapter with the analytical (BOSOR5) results. Unless noted otherwise, the tensile stress-strain curve for concrete that is used as input in the BOSOR5 analysis is the 'first approximation' curve as shown in Figs. 3.3 and 3.4 with a peak strength of 0.6 f'_t. It is shown later, in Sect. 4.4, that the BOSOR5 results vary only insignificantly as the degrading branch of the stress-strain curve is varied slightly from the first approximation. The response curve is, however, much more sensitive to the value of the peak strength. This will also be demonstrated. The compressive stress-strain curve adopted is the one proposed in Sect. 3.4.3. Furthermore, all the BOSOR5 results are based on the Form 4 yield curve as described in Ref. 14.

Segments 4 and 7 are non-prestressed and are separated from the prestressed segments in terms of discussion. No results are presented for Segment 9 which has spliced rebars that cannot be simulated by the BOSOR5 program.

4.2 Segment Properties and Modelling

Typical details of the prestressed test segment are shown in Figs. 4.1 to 4.3, and the properties of the various specimens are contained in Tables 3.1 and 3.3.

The non-prestressed segments have no prestressing strands and contain only two orthogonal layers of mild steel located near each face of each segment.

The prestressed segments contain both mild steel and prestressing strands. In the uniaxially loaded segments (Segments 5 and 6) strands are not provided in the direction in which no load is applied (the 4 tendon direction).

The method of modelling the segments for the BOSOR5 analysis has been described in Sect. 2.5.2 of Ref. 14. Briefly, each segment is modelled as a multi-layered, open-ended cylindrical shell loaded with normal pressure and line loads. To avoid confusion, it is emphasized that direction 1 represents the vertical direction of the specimen as tested in the test rig, and corresponds to the meridional direction of the BOSOR5 shell model. The orthogonal direction is referred to as direction 2. In the biaxially loaded, prestressed segments (Segments 1, 2, 3, 8 and 9), direction 1 always has 4 strands whereas the orthogonal direction has 3 strands (see Fig. 4.1).

The mild steel is simulated as an elastic-perfectly-plastic material whose properties are shown in Table 3.1.

All the BOSOR5 analyses that were carried out for the wall segments, together with the theoretical stress-strain curves for concrete, are summarized in Tables 4.1 and 4.2. It should be noted that the strain corresponding to the peak tensile stress in all the tensile stress-strain curves is kept constant at 0.00012. Whenever the strain in an analysis of a wall segment reaches 0.00012, the concrete is assumed to have cracked and this point is designated by 'C' in the figures showing the response of the segments. Similarly, the point at which the rebars yield is indicated by the symbol 'R'.

The theoretical modulus of elasticity and Poisson's ratio are assumed to be 3.8×10^6 psi and 0.2, respectively.

The concept of simulating the effects of prestressing as temperature loads, used in Ref. 14, is discarded in this report because of the difficulties in convergence encountered in the BOSOR5 execution. Instead, the effects of prestressing are simulated as external pressure and line loads acting in the opposite direction to the applied loads on the shell model. However, this method does not account for the strain differential between the concrete and the prestressing strands as shown in Fig. 2.1. Therefore, the stress-strain curves for the prestressing strands were decreased by the strain differential $|\varepsilon_{pe}|$ so that artificial origins were introduced in the curve as tabulated in Fig. 4.4

4.3 Results of Non-prestressed Segments

The experimental and analytical results of Segments 4 and 7 are compared in Figs. 4.5 and 4.6, respectively, in terms of load-strain relationships. Both segments are loaded biaxially with a load ratio of 1:1. However their physical properties are too diversified to allow direct comparison of their results. The main differences in the properties are:

	Segment No. 4	Segment No. 7
Compressive strength of concrete:	5590 psi	3290 psi
Splitting tensile strength:	536 psi	312 psi
Mild steel per layer:	8 - #4 @ 4"	6 - #6 @ 6"
Mild steel ratio per direction:	0.0097	0.0106
Segment thickness:	10.5 in	15.75 in

With the equal biaxial loading, it would be expected that the measured strains in the two loaded directions would be the same. This was not strictly true for Segment 4 as shown in Fig. 4.5, although the trends in the two directions are similar. The agreement between the two directions is excellent for Segment 7. It is seen that the BOSOR5 prediction (Run 4a in Fig. 4.5) gives lower strains than the experimental response. The discrepancy is mainly due to high tensile strength of 0.6 f_t' assumed in the BOSOR5 analysis. According to Table 3.2, the observed cracking load is estimated to be 60 kips, based on visual examination of photographs (see notes in Table 3.2). This load gives a corresponding tensile strength of 0.48 f_t'. However, the graphical procedure of crack detection gives a cracking load of 40.6 kips which produces a corresponding tensile strength of 0.32 f_t'. Therefore, a second BOSOR5 prediction using 0.32 f_t' gives a response (Run 4b in Fig. 4.8) that correlates well with the experimental response. This indicates that good predictions can be obtained if the material properties, especially the tensile strength of concrete, are known.

It can be noted that the analytical prediction overestimates the load, at the time the rebars yield, by an amount roughly equal to the residual strength of the concrete times the net area of the concrete ($\simeq$100 psi x 327.6/1000 = 32.8 kips). It would seem that the concrete in this segment degrades more rapidly than the concrete in the prestressed segments which are discussed in Sect. 4.4. Whether this conclusion is valid for all non-prestressed structural elements, or not, cannot be determined from the current series of tests because of the small number of non-prestressed segments that were tested.

Two similar analytical predictions are also given for Segment 7 in Fig. 4.6. Again Run 7a is based on 0.6 f'_t and Run 7b on the average stress at cracking. Even with the 'true' tensile strength, the measured strains are noticeably higher than the analytical strain of Run 7b at all load levels. There seems to be high extensibility in the test segment even in the pre-cracking range. It is suspected that the method of load application (see Sect. 3.3) coupled with the large size rebars widens the zone in which loads are transferred into the specimen. In this zone the surface strains may be large due to bond splitting stress. Nevertheless, the slopes of the analytical and experimental curve agree quite well, even though the magnitude of strain is considerably underestimated.

The general conclusion that can be obtained from the above observation is that the concrete in a non-prestressed segment could be degrading at a faster rate once cracking occurs leading to high extensibility in the concrete. This is seen in the derived stress-stress curves for Segments 4 and 7 in Fig. 3.4, if the mathematical derivation is accepted as reasonable.

In the analysis of a non-prestressed wall segment, the program will not converge if the rebars have yielded and if the applied loaded is increased. This is because the rebars have been simulated as an elastic-perfectly-plastic material and the wall segment cannot provide extra internal resisting forces once the rebars yield. Therefore, the BOSOR5 predictions in Figs. 4.5 and 4.6 actually terminate at the points labelled 'R', beyond which the load-strain response is

arbitrarily assumed to be horizontal. It would be possible to modify the BOSOR5 program to reduce the loading so that it continues to execute after the rebars have yielded. The resulting average strain would then continue to increase with decreasing load. Such programs are numerically sensitive and no attempt has been made to incorporate this type of solution procedure into BOSOR5.

4.4 Results of Prestressed Segments

4.4.1 Uniaxially Loaded Segments

The uniaxially loaded segments are Segments 5 and 6, with the following differences in their physical properties.

	Segment 5	Segment 6
Compressive strength of concrete	5690 psi	4540 psi
Splitting tensile strength:	444 psi	325 psi
Mild steel per layer:	10 - #3 @ 3"	8 - #4 @ 4"
Mild steel ratio per direction:	0.0067	0.0097

Three sets of analytical results (Runs 5a, 5b and 5c in Fig. 4.7) are given for Segment 5. Run 5a is based on $f_t'' = 0.6\ f_t'$ and the first approximate tensile stress-strain curve, whereas Run 5b is also based on $f_t'' = 0.6\ f_t'$ but with the 'proposed' tensile stress-strain curve (i.e., the second approximations of Fig. 3.3). The two curves are very similar except that the load at which the rebars yield is slightly higher for Run 5b than that for Run 5a (by about 1.7 percent). This shows that a slight variation in the degrading branch of the tensile stress-strain curve does not significantly affect the results of the analysis.

Run 5c is based on $f_t'' = 0.88\ f_t'$ and the 'proposed' stress-strain curve where $0.88\ f_t'$ is the computed tensile strength of the concrete in this segment. This curve agrees reasonably well with the experimental results except at high loads. The actual test segment seems to be stiffened at the high loads as shown by the response a-b in Fig. 4.7. The response beyond point 'a' occured during a reloading process which seems to cause a stiffening of the concrete. If point 'a' is joined to point 'c' on the experimental curve, the slopes of the experimental and analytical curve are parallel.

For Segment 6, the BOSOR5 analysis predicts lower strains than measured (see Fig. 4.8). However the comparison is reasonable.

4.4.2 Biaxially Loaded Segments

Consider first Segment 3 having a load ratio of 1:1 which was maintained only up to a load of 375 kips. Subsequently, the direction 2 load was held constant at 375 kips and the direction 1 load was increased until the termination of the test. The experimental and analytical load-strain curves for this segment are shown in Fig. 4.9. It is seen that the BOSOR5 analysis predicts the response well in direction 2 but slightly underestimates the stiffness in the orthogonal direction.

Segments 1 and 8 were tested with a load ratio of 1:2. Both basically had similar physical properties except for the concrete cover which was 0.5 in. in Segment 1, and 1.25 in. in Segment 8. The BOSOR5 analysis for Segment 1 (see Fig. 4.10) predicts the strains very effectively in the direction of maximum strains, but yields somewhat a stiffer response in the orthogonal direction.

The experimental and analytical load-strain curves for Segment 8 are shown in Fig. 4.11. It is seen that the analytical curve, based on an assumed tensile strength of 0.6 f_t' of the concrete (Run 8a), agree well with the experiment curve for direction 1, although the 'true' tensile strength is 0.76 f_t'. Using the latter tensile strength for a better analytical prediction would slightly shift the analytical response to the left of Run 8a, but the ultimate load would remain the same. Agreement is not obtained for direction 2. A similar trend is seen as for Segment 1 (Fig. 4.10) indicating that the measured strains in Segments 1 and 8 are consistent and reliable. This suggests that if a more accurate prediction is required in the direction 2, the analytical yield function used in BOSOR5 needs to be revised. However, it is the authors' opinion that sufficient correlation is at least obtained in the major direction and revision is not warranted at this time.

A second analytical prediction is obtained using the proposed stress-strain curve of Sect. 3.4.3 and is shown as Run 8b in Fig. 4.11. The deviation from Run 8a in direction 1 is small, whereas the deviation in direction 2 cannot be seen. This again shows that the analytical prediction is not significantly changed by varying slightly the degrading branch of the stress-strain curve of concrete. It has been found that the choice of the theoretical degrading branch, within the proximity of the proposed form, is governed by the ease with which the program executes. For convergence in BOSOR5, the loss in the concrete stiffness (AE) must be no greater than the stiffness of the reinforcement during any load step. Assurance that convergence will occur after rebar yield

can only be guaranteed by preliminary manual calculations and with experience in the use of the BOSOR5 program.

4.5 Effects of the Shape of the Tensile Stress-Strain Curve on BOSOR5 Execution

Slight variations in the shape of the degrading branch of the tensile stress-strain of concrete do not significantly affect the BOSOR5 results, as shown in Sect. 4.4. However, the shape affects the ease with which the BOSOR5 program executes and hence, it affects the execution cost.

A comparison of the execution times is given in Table 4.3 for Segment 5 in terms of the CPU time required by the FLOW3 subroutine which calculates the updated properties of the concrete. The three different BOSOR5 runs in Table 4.3 are based on a tensile strength of 0.6 f_t' (f_t' = 444 psi) but with different degrading branches in the stress-strain curve. Run 5a is based on the type 1 stress-strain curve shown in Table 4.1, whereas Run 5b is based on type 2. Run 5d has a stress-strain curve identical to that of Run 5b except that there are fewer callout points for the input curve; that is, callout points 4, 6, 8 and 9 (see diagram in Table 4.1) have been eliminated.

Comparing the CPU times of Runs 5a and 5b, the following observations can be made:

(1) At load step 10, the rebars have yielded in both the runs and the accumulated CPU times between them are comparable.

(2) Beyond load step 10, the concrete in Run 5a is in the horizontal degrading branch of the stress-strain curve, implying that its

stiffness has stabilised. Therefore, relatively large load increments are possible beyond load step 10 since the negative stiffness of the concrete is easily compensated for by the positive stiffness of the reinforcement. On the other hand, the concrete in Run 5b is still degrading relatively fast and hence, the load increment has to be decreased, owing to convergence difficulties in the analysis.

(3) Beyond load step 10, the CPU time per load step increases dramatically in Run 5b.

(4) At the termination of the runs, the ratio of accumulated CPU times is: - Run 5a/Run 5b = 138.80 secs./202.33 secs. (or 1:1.46). Although the termination loads are not the same, the total strains are similar and equal to 0.014. The difference in the CPU times is effectively higher due to the additional load increments in Run 5b, which means higher CPU virtual memory storage cost, which could amount to 40 percent of the total execution cost.

The CPU time in Run 5b could effectively be reduced by specifying fewer callout points for the input stress-strain curve, as shown by Run 5d in Table 4.3. Moreover, the simpler curve permits larger load increments towards the end of the run.

The general conclusion is that the stress-strain curve should be simulated with as few linear segments as possible. The execution cost increases significantly as the rate of degradation of concrete stress is increased.

5. CONCLUSIONS

A tensile stress-strain curve for concrete has been derived for use with the three-parameter theory. The curve has a degrading branch very similar to the well-established curve for compression. The maximum tensile strength of the concrete in the test segments is found to have an average value of 0.6 f'_t or 3.65 $\sqrt{f'_c}$. This low value results from the rate of loading and the effect of volume.

The uniaxial tensile stress-strain curve recommended for use with the three parameter elastic-plastic hardening theory for the simulation of the response of uniaxially and biaxially loaded prestressed concrete segments is the one shown in Fig. 3.8 with a peak stress of $f''_t = \alpha f''_t$. For computation purposes this curve may be approximated by a series of straight lines.

For prestressed concrete wall segments a value of α of 0.6 is recommended. For analysis of larger structures, slowly loaded, such as the U of A. test structure, a value of α of 0.5 is recommended. For applications to prototype structures, which are significantly larger, and are loaded at a more rapid rate, Table 3.4 indicates that a value of α of 0.6 would be the best estimate available on the basis of existing data.

On the basis of two biaxially loaded nonprestressed reinforced concrete segments, no firm recommendation for α can be made but it appears that a value of approximately one half of that for prestressed segments would be appropriate.

REFERENCES

1. ACI Code, "Building Code Requirements for Reinforced Concrete (ACI Standard 318-71)", American Concrete Institute, P.O. Box 4754, Redford Station, Detroit, Michigan, 48219.

2. ACI Committee Report, "Commentary on Building Code Requirements for Reinforcement Concrete (ACI 318-71)", American Concrete Institute, P.O. Box 4754, Redford Station, Detroit, Michigan, 48219.

3. Bolotin, V.V., "Statistical Methods in Structural Mechanics", Holden-Day, Inc. 1969.

4. Bushnell, D., "BOSOR5 - A Computer Program for Buckling of Elastic-Plastic Complex Shells of Revolution Including Large Deflections and Creep; Vol. 3: Theory and Comparisons with Tests", Lockheed Missiles and Space Company, Inc., Sunnyvale, California, Dec., 1974.

5. Comité Européen du Béton, "Proposed Complements to the CEB-FIP International Recommendations of 1970", CEB Bulletin d'Information No. 74, March 1972.

6. Evans, R.H., and Marathe, M.S., "Microcracking and Stress-Strain Curves for Concrete in Tension", Materials and Structures, Vol. 1, No. 1, Jan.-Feb., 1968, pp. 61-64.

7. Hognestad, E., "A Study of Combined Bending and Axial Load in Reinforced Concrete Members", Bulletin Series No. 399, University of Illinois Experiment Station, Vol. 49, No. 22, November, 1951.

8. Hughes, B.P., and Chapman, G.P., "The Complete Stress-Strain Curve for Concrete in Direct Tension", Bulletin RILEM No. 30, March, 1966, pp. 95-97.

9. Kupfer, H., Hilsdorf, H.K. and Rüsch, H., "Behavior of Concrete under Biaxial Stresses", Journal of the American Concrete Institute, Vol. 66, No. 8, Aug., 1969, pp. 656-666.

10. Linder, C.P. and Sprague, J.C., "Effect of Depth upon the Modulus of Rupture of Plain Concrete", Proc. American Soc. for Testing of Materials, V. 55, 1955, pp. 1062-1075.

11. Malhotra, V.M., "Effect of Specimen Size on Tensile Strength of Concrete", Journal of the American Concrete Institute, Vol. 67, No. 6, June, 1970, pp. 467-469.

12. McNeely, D.J., and Lash, S.D., "Tensile Strength of Concrete", Journal of the American Concrete Institute, Vol. 60, No. 6, June, 1963, pp.751-761.

13. Mirza, S.A., Hatzinikolas, M., and MacGregor, J.G., "Statistical Descriptions of the Strength of Concrete", Submitted for Publication to the Structural Division, ASCE.

14. Murray, D.W., Chitnuyanondh, L., Wong, C., and Rijub-Agha, K.Y., "Inelastic Analysis of Prestressed Concrete Secondary Containments", Structural Engineering Report 67, Department of Civil Engineering, University of Alberta, Edmonton, Alberta, Canada, July, 1978.

15. Neville, A.M., "Properties of Concrete", Second Edition, Pitman Publishign Cooperation, 6 East 43 Street, New York, N.Y., 10017, 1973.

16. Orangun, C.O., Jira, J.O., and Breen, J.E., "A Reevaluation of Test Data on Development Length and Splices", Journal of the American Concrete Institute, Vol. 74, No. 3, March, 1977, pp. 114-122.

17. Popovics, S., "A Review of Stress-Strain Relationships for Concrete", Journal fo the American Concrete Institute, Vol. 67, No. 3, March, 1970.

18. Sargin, M., "Stress-Strain Relationships for Concrete and the Analysis of Structural Concrete Sections", Study Series No. 4, Solid Mechnaics Division, University of Waterloo, Waterloo, Ontario, Canada, 1971.

19. Tasuji, M.E., Slate, F.O., and Nilson, A.H., "Stress-Strain Response and Fracture of Concrete in Biaxially Loading", Journal of the American Concrete Institute, Vol. 75, No. 7, July, 1978, pp. 306-312.

TABLES

Table 3.1 - Properties of Wall Segments

1	2	3	4	5	6	7	8
Specimen Number	Prestressing	Load Ratio H:V	Nominal Thickness in.	Nominal Concrete Cover in.	Mild Steel Properties†		
					Bars per Layer	Yield Strength ksi	E x 10^6 psi
4	none	1:1	10.5	0.5	8 - #4 @ 4"	53.5	29.3
7	none	1:1	15.75	0.75	6 - #6 @ 6"	52.9	28.5
5	1 - dir.	1:0	10.5	0.5	10 - #3 @ 3"	60.0	28.5
6	1 - dir.	1:0	10.5	0.5	8 - #4 @ 4"	55.0	29.3
3	2 - dir.	1:1	10.5	0.5	10 - #3 @ 3"	60.0	28.5
1	2 - dir.	1:2	10.5	0.5	10 - #3 @ 3"	60.0	28.5
2	2 - dir.	1:2	10.5	0.5	10 - #3 @ 3"	60.0	28.5
8	2 - dir.	1:2	10.5	1.25	10 - #3 @ 3"	58.2	28.9
9*	2 - dir.	1:2	10.5	0.5	10 - #3 @ 3"	60.0	28.5

† The yield strengths and the moduli of elasticity are the ones used for BOSOR5 analysis and they may vary slightly from the final experimental values.

* Segment 9 had spliced bars and will not be used in derivation of stress-strain curve.

Table 3.2 - Observed Cracking Loads in Wall Segments

Specimen Number	Vert. Load at Cracking, kip*		Horiz. Load at Cracking, kip*		Overall Load at Cracking, kip **	
	Face A	Face B	Face A	Face B	Vert.	Horiz.
4	80.3	60.0***	60.0	60.0	60.0	60.0
7	75.1	100.0	82.1	82.1	75.1	82.1
5	--	--	280.2	255.5	--	267.0
6	--	--	185.0	196.0	--	185.0
3	350.0	300.0	206.8	206.8	330.0	206.8
1	300.0	325.0	194.0	179.3	320.0	179.3
2	287.5	300.0	183.5	200.0	287.5	191.75
8	350.0	350.0	175.0	175.0	350.0	175.0
9	350.0	300.0	181.8	181.8	300.0	181.8

* The vertical load at cracking is the value of the vertical load when horizontal cracks formed. The horizontal load at cracking is the horizontal load when vertical cracks formed.

** The overall cracking loads are the values of vertical load (or horizontal) when the average load-strain relationships changed slope.

*** The graphical procedure detected cracks at 40.6 kips, however, the first visual observation of cracking was between 60.0 and 80.0 kips. Also, during this load increment, cracks crossed the strain gages mounted on the surface. The cracking load has been estimated to be 60.0 kips.

Table 3.3 Measured and Computed Strengths of Concrete of Wall Segments

1	2	3	4	5	6	7	8	9	10	11
Specimen Number	Prestressing	Cylinder Strengths, psi			Estimated[1] Cracking Load, kip	Computed tensile Strength, psi[2]		$\frac{f''_t}{f'_t}$	$\frac{f''_t}{\sqrt{f'_c}}$	Meas. Strain at First Crack x 10^{-6}
		f'_t	f'_c	$f'_t/\sqrt{f'_c}$		f''_t	f_{to}			
4	none	536	5590	7.17	60 (1)	256	171	0.48	3.42	80
7[4]	none	312	3290	5.44	75.1(1)	168	142	0.54	2.93	300
5	1 - dir.	444	5690	5.89	255.5(2)	389	374	0.88	5.16	170
6	1 - dir.	325	4540	4.81	185.0(2)	223	139	0.69	3.31	160
3	2 - dir.	426	5690	5.63	206.8(2)	229	193	0.54	3.04	190
1	2 - dir.	490	5090	6.87	300.0(1)	307	225	0.63	4.30	370
2	2 - dir.	436	4460	6.53	287.0(1)	174	136	0.40	2.61	90
8	2 - dir.	424	4920	6.05	350.0(1)	321	308	0.76	4.58	390
9	2 - dir.	437	3920	6.98	300.0(1)	221	176	0.51	3.53	--
				6.15	= MEAN =			0.60	3.65	220[3]
				0.79	= STANDARD DEVIATION =			0.15	0.85	120
				0.13	= COEFF. OF VARIATION =			0.25	0.23	0.55

1. The number in parentheses denotes the direction which cracks first appeared, i.e. (1) refers to horizontal cracks (due to vertical loads), whereas (2) refers to vertical cracks (due to horizontal loads).
2. f''_t and f_{to} are computed with and without bending moments, respectively.
3. The average in col. 11 is computed without segment 9 which has spliced rebars.
4. Specimen 7 contains 2 batches of concrete, the strengths in columns 3 and 4 are for the face on which the cracks started.

Table 3.4 Derived Tensile Strengths for Various Types of Applications

(1) Type of Application	(2) Volume Effect	(3) Ratio Effect	(4) Theoretical* α = (2) x (3)	(5) Effective α
(a) Wall segments				
- uniform stress	.60	.89	.53	.60
- flexural stress	.68	.89	.61	--
(b) U. of A. Test Structure	.48	.87	.42	.50
(c) Accidental Overload of a Prototype	.48	1.17	.56	--

*$f''_t = \alpha f'_t$, where f'_t = tensile strength of 6 x 12 cylinder as measured by a Brazilian tensile test.

Table 4.1 Tensile Stress-Strain Curves used for BOSOR5 Analysis

Specimen No.	Type of* $\sigma - \varepsilon$ Curve	$\alpha = \frac{f''_t}{f'_t}$	$\sigma - \varepsilon$ curve*			BOSOR5 Results
			Point on Curve	σ, psi	$\varepsilon \times 10^{-3}$	
4	1	0.6	1	0.0	0.0	See Run 4A
			2	145.0	0.0382	in Fig. 4.5
			3	322.0	0.12	
			4	306.0	0.3	
			5	60.0	2.2	
			6	10.0	100.0	
	1	0.48	1	0.0	0.0	See Run 4B
			2	77.8	0.0205	in Fig. 4.5
			3	172.9	0.12	
			4	164.0	0.3	
			5	60.0	2.2	
			6	10.0	100.0	
7	1	0.6	1	0.0	0.0	See Run 7A
			2	84.2	0.0222	in Fig. 4.6
			3	187.0	0.12	
			4	177.7	0.3	
			5	60.0	2.2	
			6	10.0	100.0	
	1	0.54	1	0.0	0.0	See Run 7B
			2	75.8	0.01995	in Fig. 4.6
			3	168.5	0.12	
			4	160.0	0.3	
			5	60.0	2.2	
			6	10.0	100.0	
5	1	0.6	1	0.0	0.0	See Run 5A
			2	119.7	0.0315	in Fig. 4.7
			3	266.0	0.12	
			4	252.7	0.3	
			5	60.0	2.2	
			6	10.0	100.0	
	2	0.6	1	0.0	0.0	See Run 5B
			2	119.7	0.0315	in Fig. 4.7
			3	266.0	0.12	
			4	252.7	0.3	
			5	135.7	1.5	
			6	76.9	2.8	
			7	52.5	3.9	
			8	31.7	6.0	
			9	22.6	10.0	
			10	5.0	1000.0	

Table 4.1 Continued

Specimen No.	Type of* $\sigma - \varepsilon$ Curve	$\alpha = \frac{f''_t}{f'_t}$	$\sigma - \varepsilon$ curve*			BOSOR5 Results
			Point on Curve	σ, psi	$\varepsilon \times 10^{-3}$	
5	2	0.88	1	0.0	0.0	See Run 5C in Fig. 4.7
			2	175.1	0.0461	
			3	389.0	0.12	
			4	369.6	0.3	
			5	198.5	1.5	
			6	112.5	2.8	
			7	76.8	3.9	
			8	46.4	6.0	
			9	33.1	10.0	
			10	7.3	100.0	
6	1	0.6	1	0.0	0.0	See Run 6A in Fig. 4.8
			2	87.8	0.0231	
			3	195.0	0.12	
			4	185.3	0.3	
			5	60.0	2.2	
			6	10.0	100.0	
1	1	0.6	1	0.0	0.0	See Run 1A in Fig. 4.9
			2	132.0	0.0345	
			3	294.0	0.12	
			4	280.0	0.3	
			5	60.0	2.2	
			6	10.0	100.0	
3	1	0.6	1	0.0	0.0	See Run 3A in Fig. 4.10
			2	114.0	0.03	
			3	254.0	0.12	
			4	241.0	0.3	
			5	60.0	2.2	
			6	10.0	100.0	
8	1	0.6	1	0.0	0.0	See Run 8A in Fig. 4.11
			2	114.0	0.03	
			3	254.0	0.12	
			4	241.0	0.3	
			5	60.0	2.2	
			6	10.0	100.0	
	2	0.6	1	0.0	0.0	See Run 8B in Fig. 4.11
			2	114.0	0.03	
			3	254.0	0.12	
			4	243.6	0.3	
			5	129.5	1.5	
			6	73.4	2.8	
			7	50.0	3.9	
			8	30.2	6.0	
			9	21.6	10.0	
			10	4.3	100.0	

Table 4.1 Continued

* The types of the tensile σ - ε curve used are:

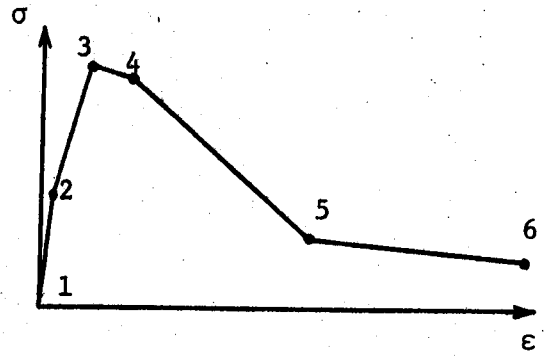

Type 1: 1st approximation in Fig. 3.4

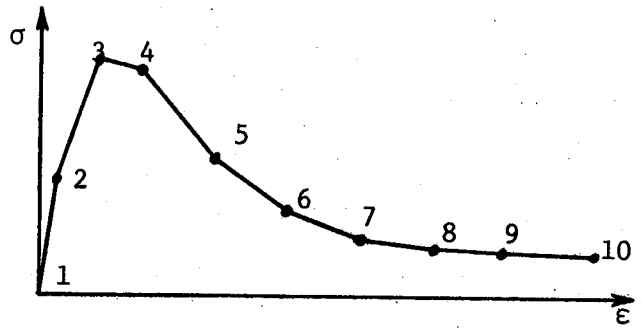

Type 2: Proposed (same as 2nd approximation in Fig. 3.4)

Table 4.2 Compressive Stress-Strain Curves used for BOSOR5 Analysis

Specimen No.	Point on Curve	σ, psi	ε x 10^{-3}
4	1	0.0	0.0
	2	2400.0	0.6316
	3	4646.0	1.8
	4	5330.0	2.805
	5	1000.0	5.0
	6	20.0	150.0
7	1	0.0	0.0
	2	1454.0	0.3826
	3	2828.0	1.1
	4	3230.0	1.7
	5	700.0	5.0
	6	20.0	150.0
5	1	0.0	0.0
	2	2354.0	0.6195
	3	4603.0	1.8
	4	5230.0	2.753
	5	1000.0	5.0
	6	20.0	150.0
6	1	0.0	0.0
	2	1881.0	0.495
	3	3757.0	1.5
	4	4180.0	2.2
	5	800.0	5.0
	6	20.0	150.0
1 & 3	1	0.0	0.0
	2	1904.0	0.501
	3	3637.0	1.5
	4	4230.0	2.4
	5	1000.0	5.0
	6	20.0	150.0
8	1	0.0	0.0
	2	2039.0	0.5366
	3	3728.0	1.5
	4	4530.0	2.3842
	5	1000.0	5.0
	6	20.0	150.0

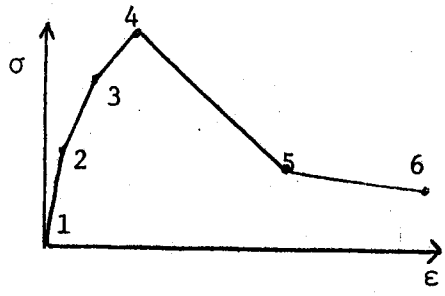

σ @ point 4

$= 0.92\ f'_c$

$E_c = 57{,}000\sqrt{f'_c}$ for both tension and compression

Table 4.3 Comparison of BOSOR5 Execution Time using Different Tensile Stress-Strain for Concrete

Load Step No.	BOSOR5 Run 5a*			BOSOR5 Run 5b*			BOSOR5 Run 5 **		
	Total Load, kip	CPU Time, sec.	Accum. CPU Time, sec.	Total Load, kip	CPU Time, sec.	Accum. CPU Time, sec.	Total Load, kip	CPU Load, sec.	Accum. CPU Time, sec.
1	133.6	0.02	0.02	133.6	0.02	0.05	133.6	0.02	0.02
2	165.1	0.22	0.24	165.1	0.23	0.25	165.1	0.21	0.23
3	196.6	3.52	3.76	196.6	3.55	3.80	196.6	3.57	3.80
4	212.4	2.17	5.93	212.4	2.21	6.01	212.4	2.20	6.00
5	228.1	2.19	8.12	228.1	2.23	8.24	228.1	2.21	8.21
6	243.9	4.55	12.67	243.9	4.61	12.85	243.9	4.49	12.70
7	275.4	7.79	20.46	275.4	80.6	20.91	275.4	4.82	17.52
8	306.9	4.91	25.37	306.9	4.98	25.89	306.9	4.97	22.49
9	338.4	4.85	30.22	338.4	6.90	32.79	338.4	6.32	28.81
10	369.9	10.68	40.90	369.9	6.26	39.05	369.9	3.78	32.59
11	398.5	23.73	64.63	380.9	11.52	50.57	401.4	46.27	78.86
12	424.5	74.17	138.80	391.9	16.58	67.15	424.5	105.01	183.87
13	--	--	--	402.3	60.86	128.01			
14	--	--	--	412.7	74.32	202.33			

* Run 5a is based on the type 1 σ-ε curve in Table 4.1, whereas Run 5b is based on type 2.

** The tensile strain-strain curve of Run 5d is the same as that of Run 5b except that the degrading branch of the curve contains fewer breaks, that is, points 4, 6, 8 and 9 of the type 2 curve in Table 4.1 are eliminated.

FIGURES

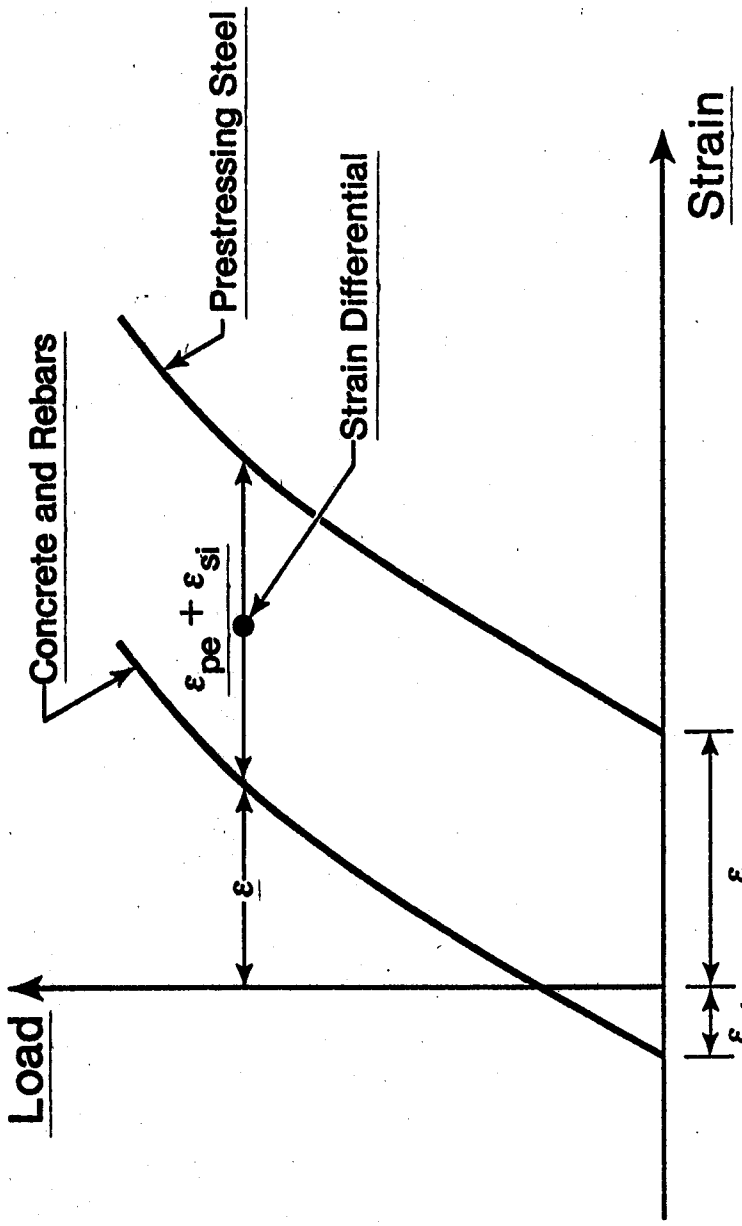

Figure 2.1 - Typical Load-Strain Response of Prestressed Concrete

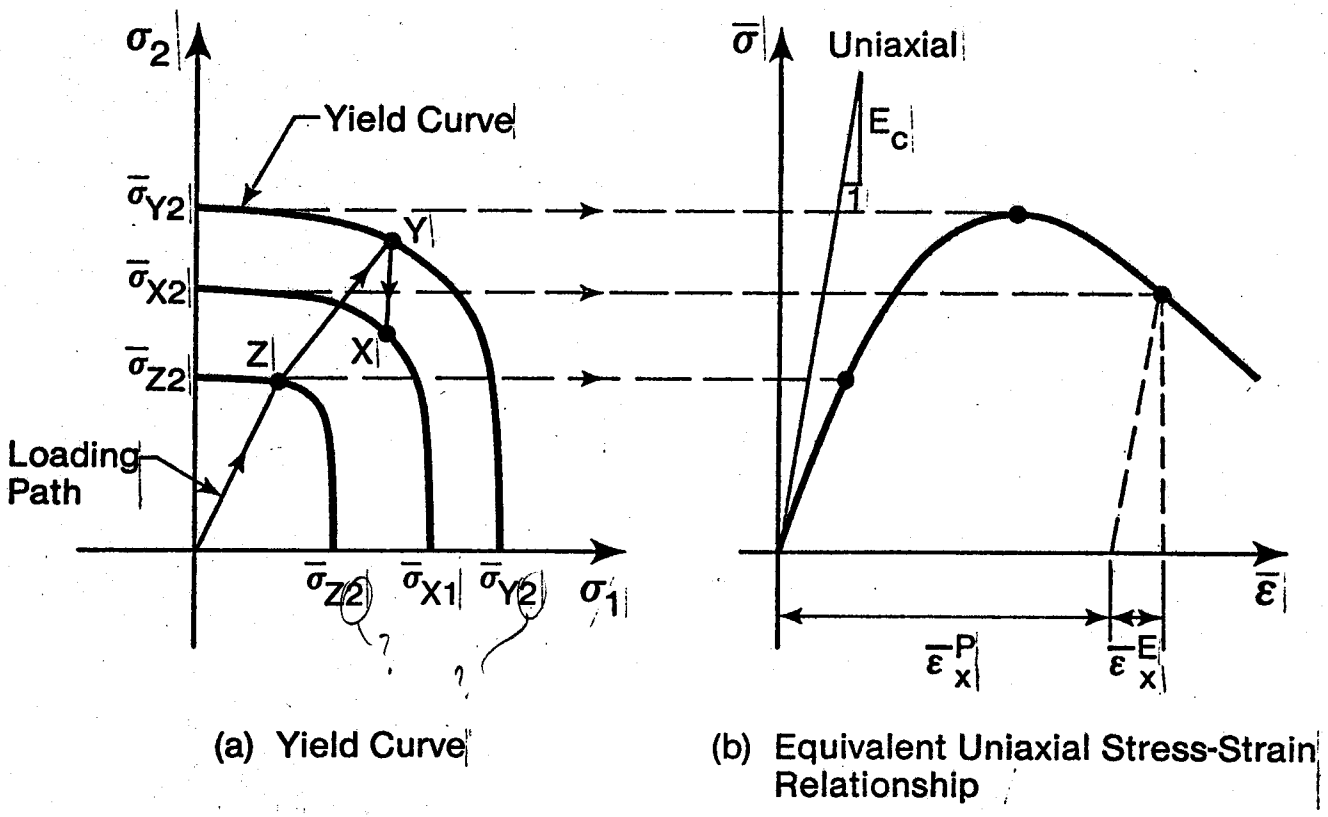

(a) Yield Curve

(b) Equivalent Uniaxial Stress-Strain Relationship

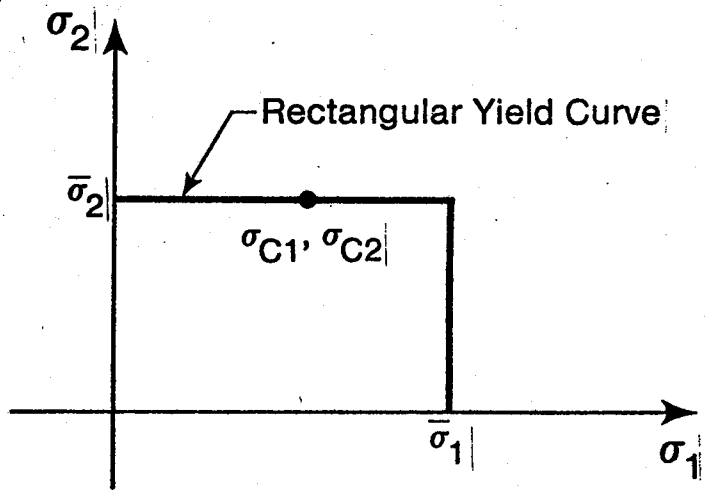

(c) Assumed Rectangular Yield Curve

Figure 2.2 - Equivalent Uniaxial Stress-Strain Relationship for Concrete.

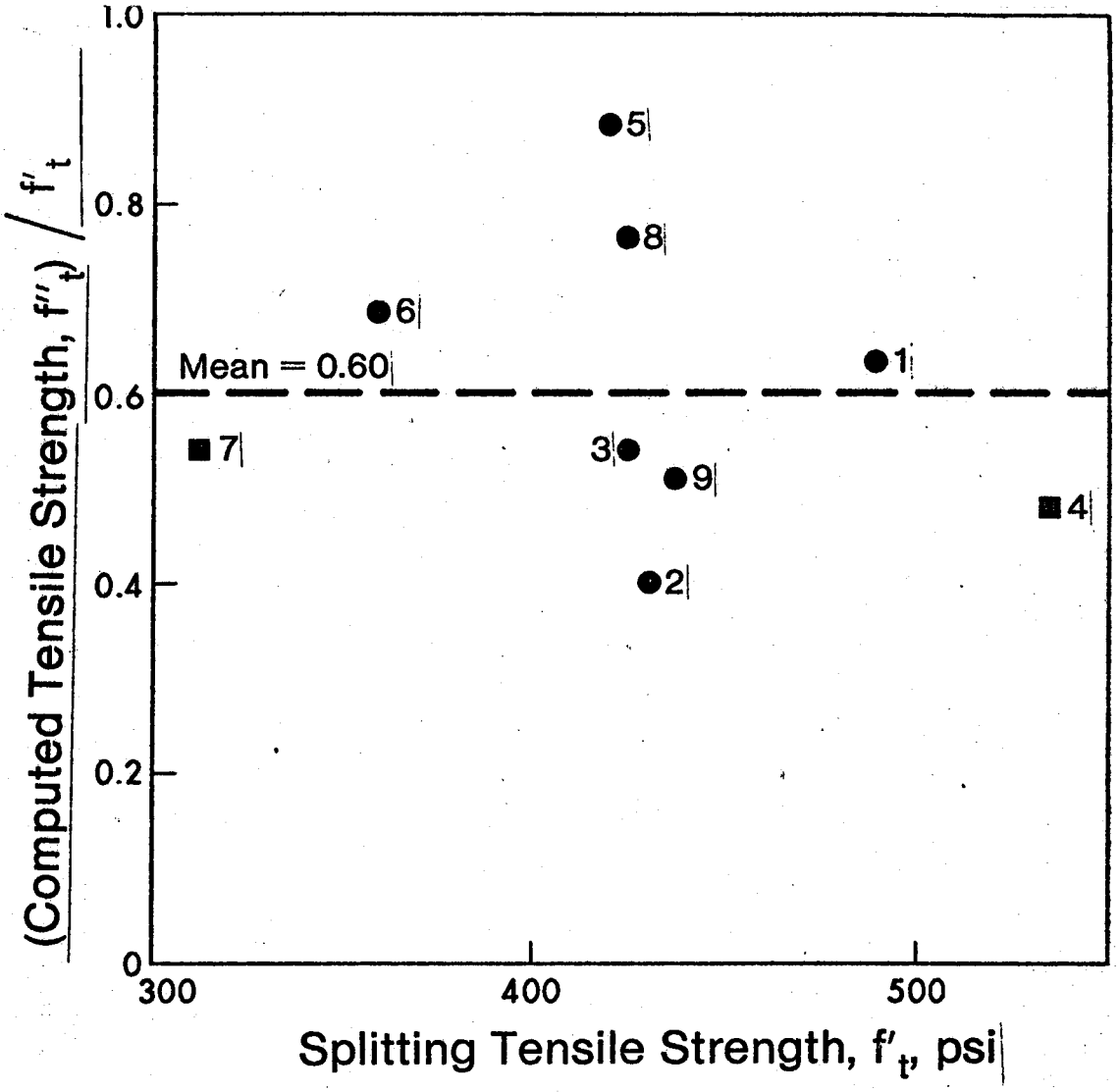

(a) Relationship Between f''_t and f'_t

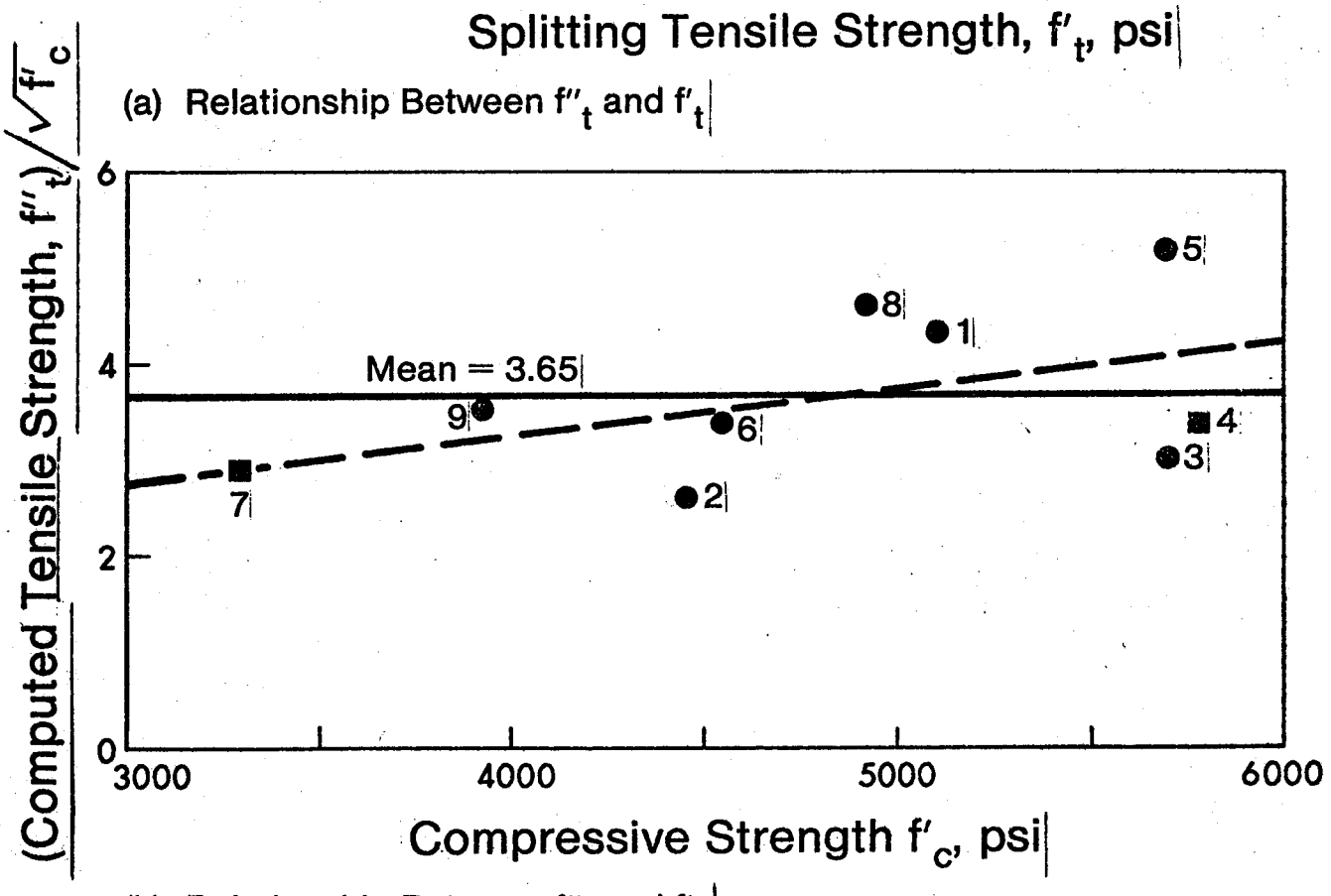

(b) Relationship Between f''_t and f'_c

Figure 3.1 - Relationship Between the Computed Tensile Strengths and

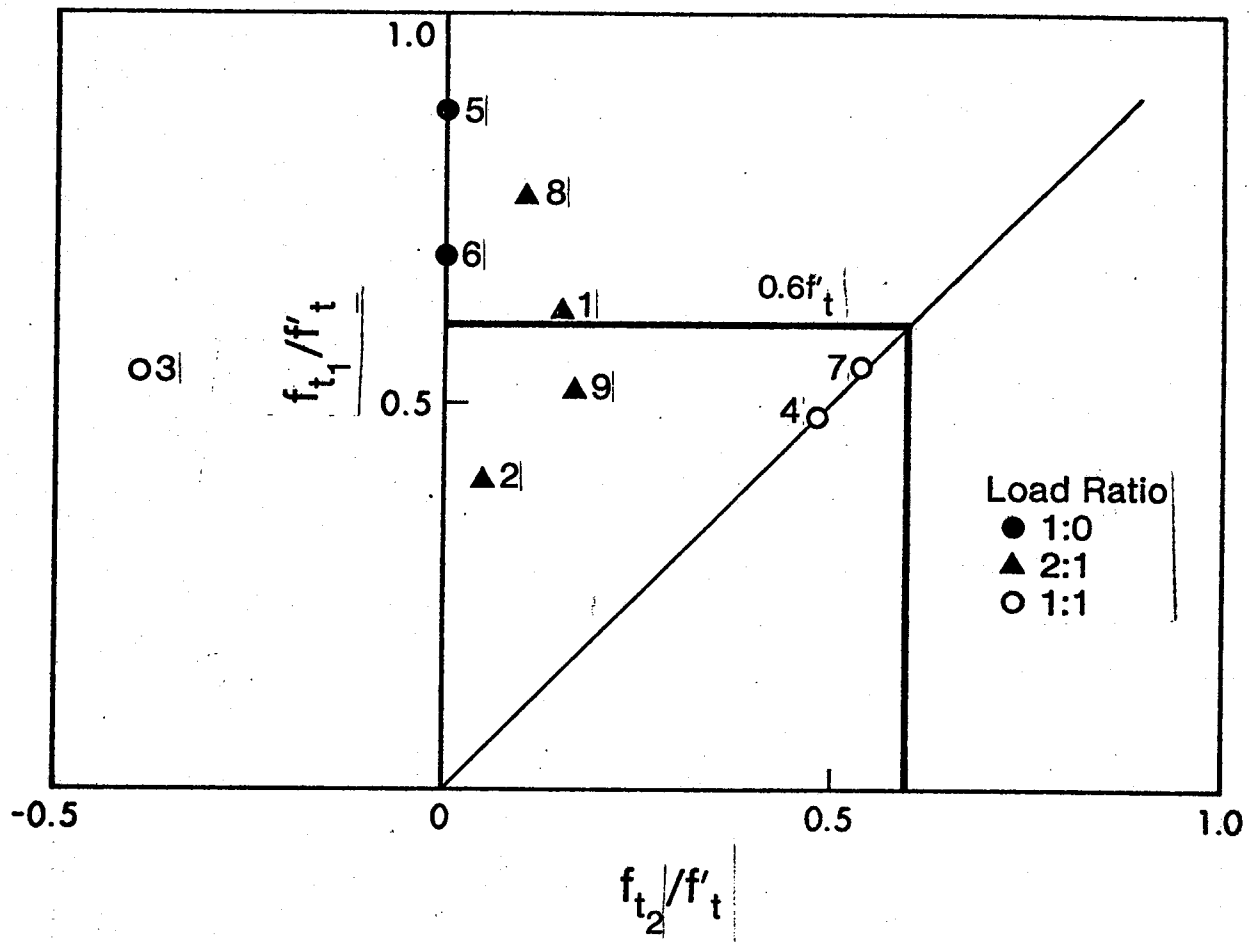

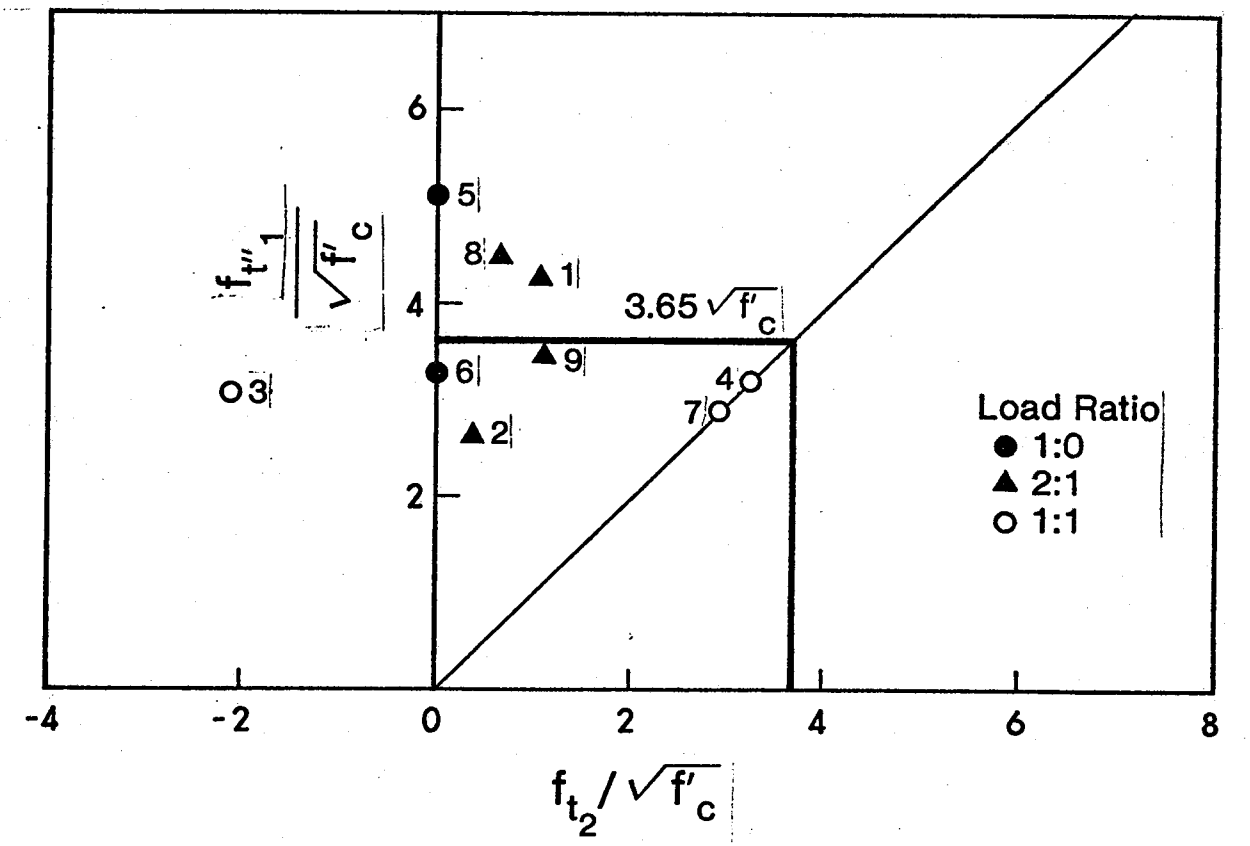

Figure 3.2 - Effect of Biaxial Stresses on Strength at Cracking.

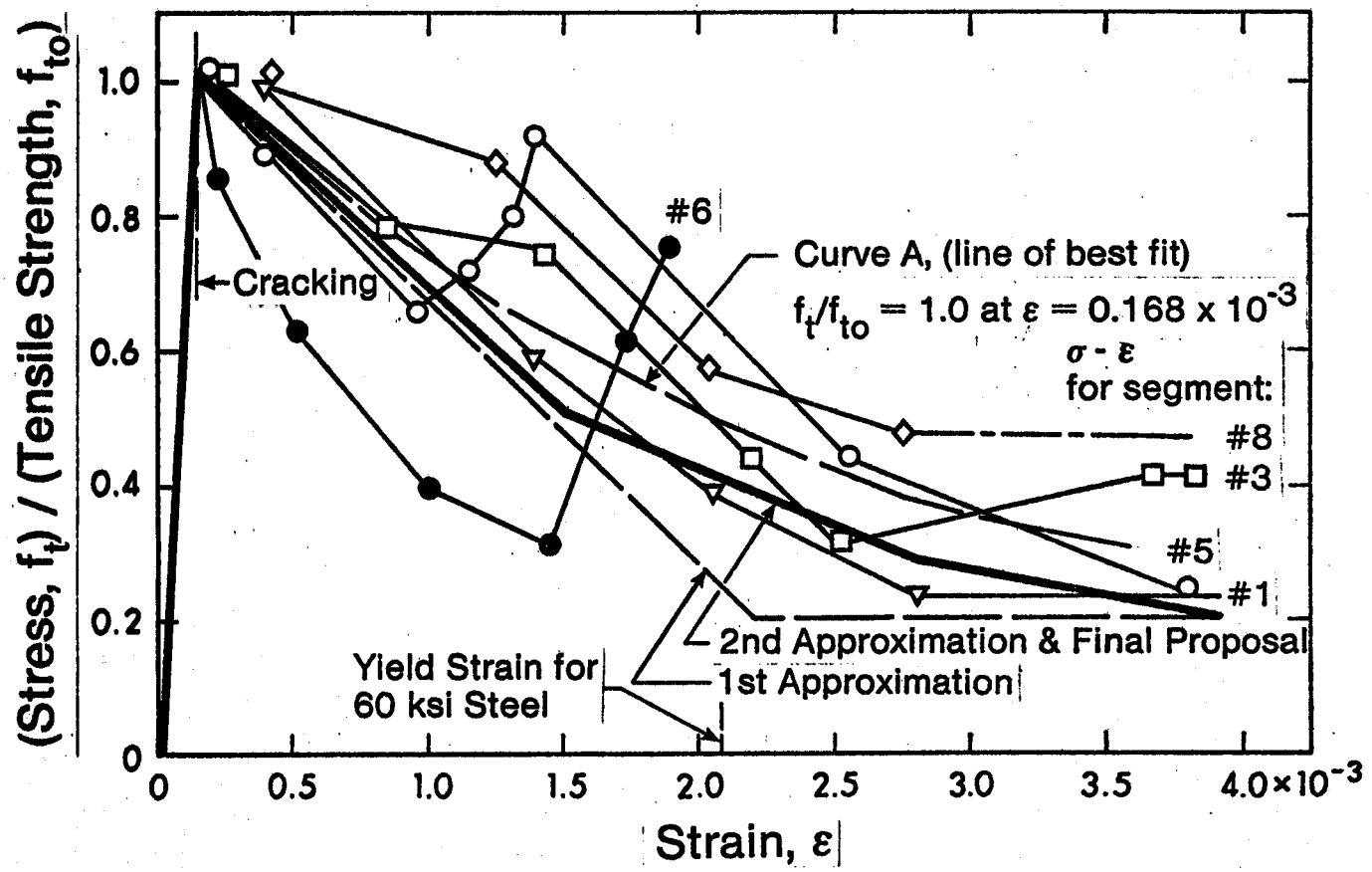

Figure 3.3 - Uniaxial Tensile Stress-Strain Curves for Prestressed Concrete

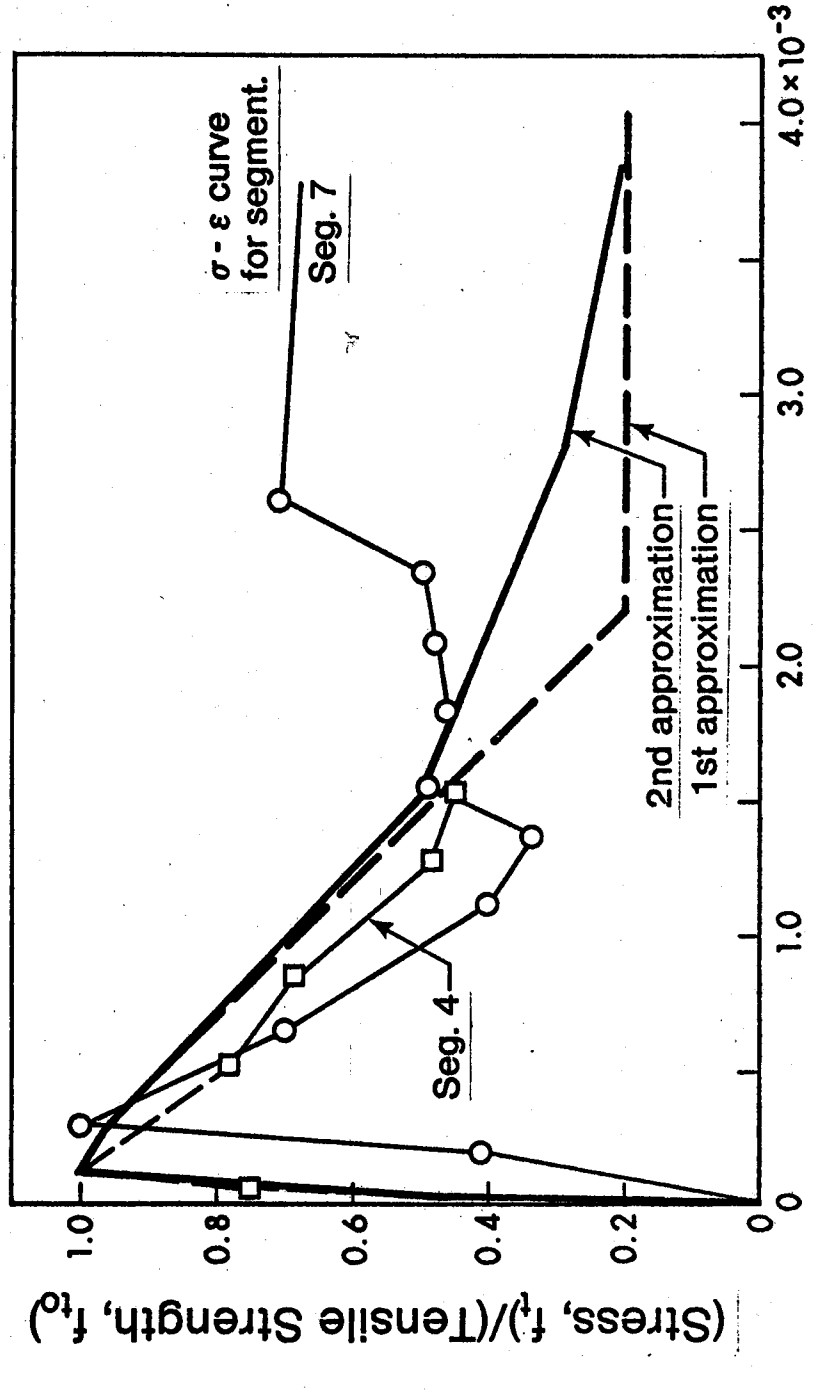

Figure 3.4 - Uniaxial Tensile Stress-Strain Curves for Nonprestressed Concrete.

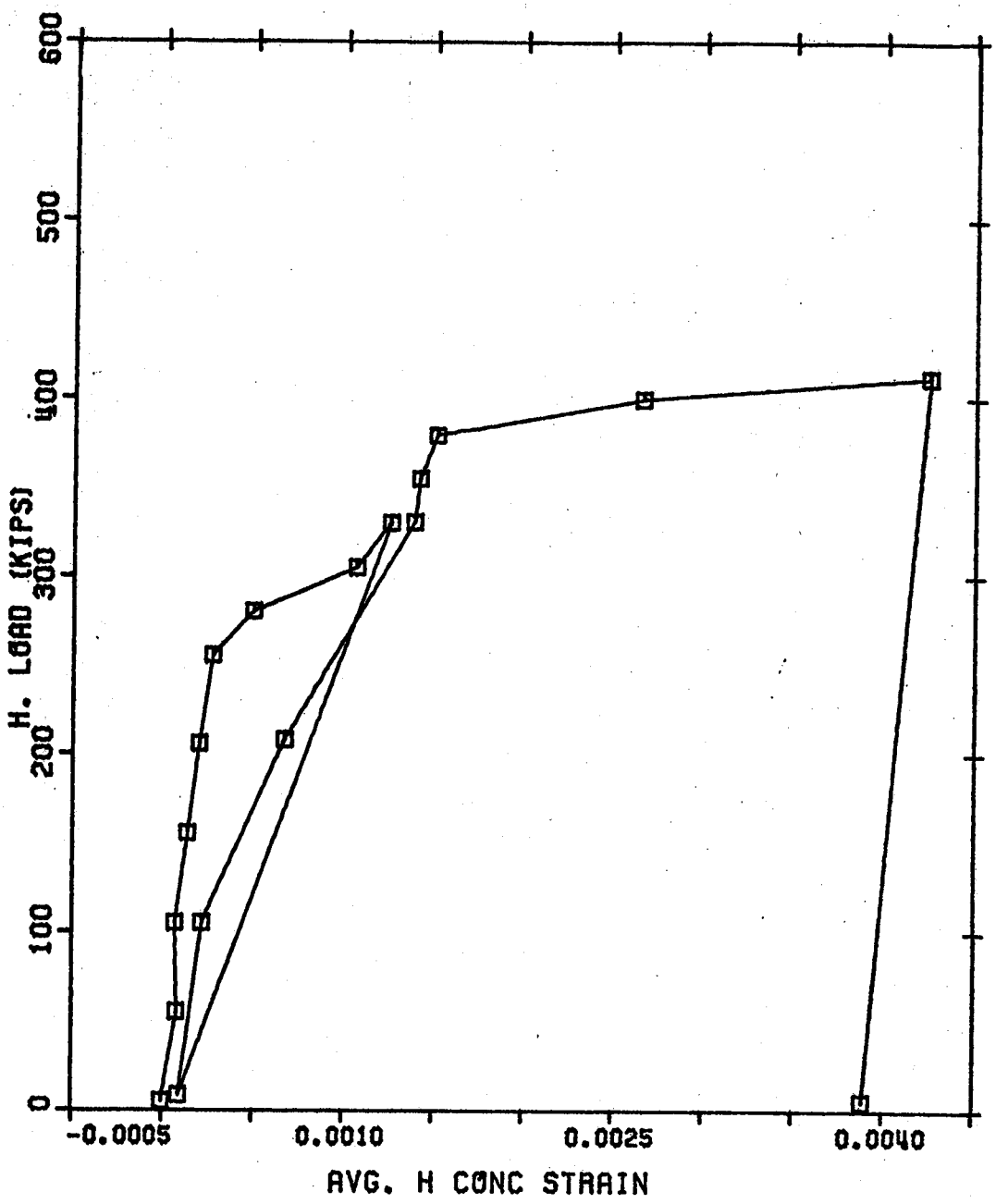

Figure 3.5 Typical Load-Strain Response of Segment 5

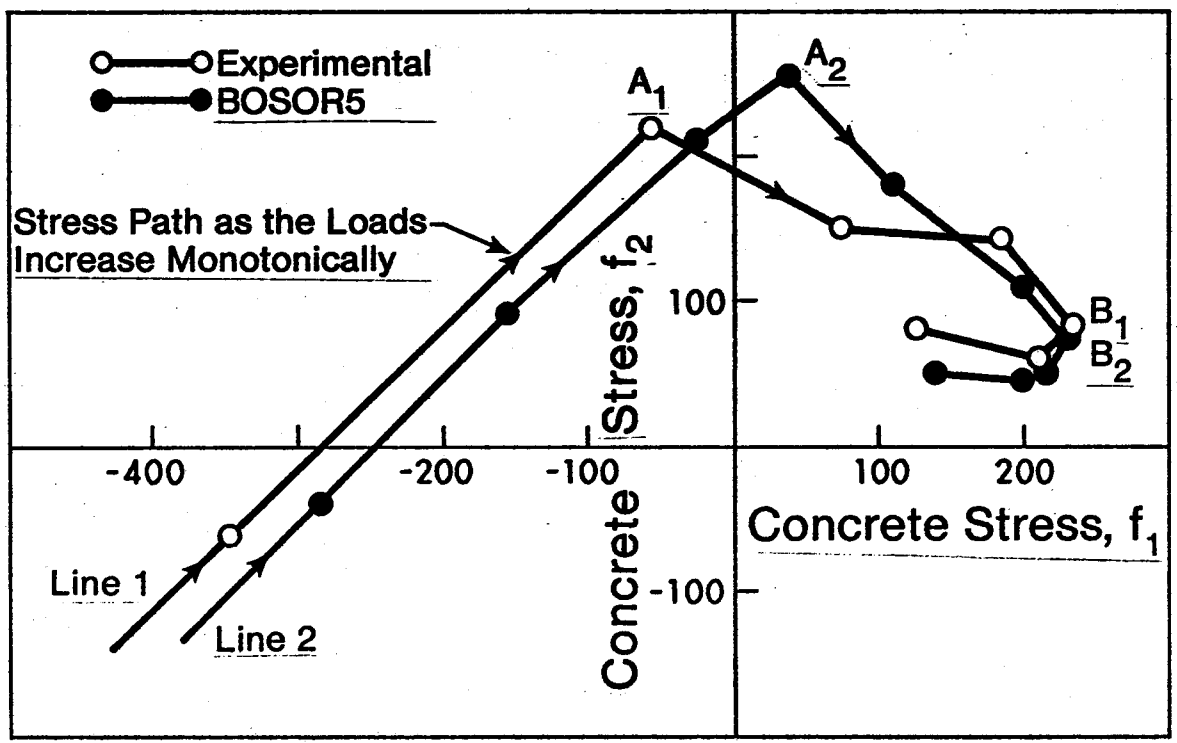

Figure 3.6 - Stress Path of Segment 3.

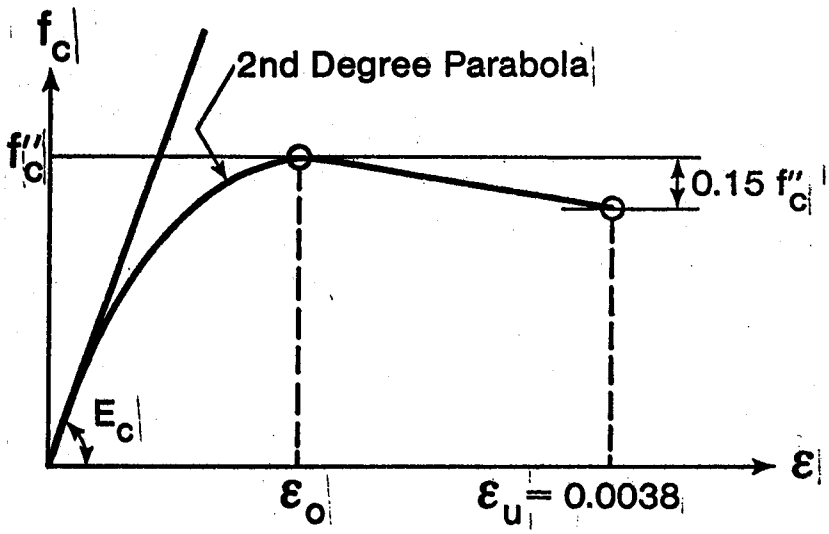

Figure 3.7 - Proposed Compressive Stress-Strain Curve for Concrete

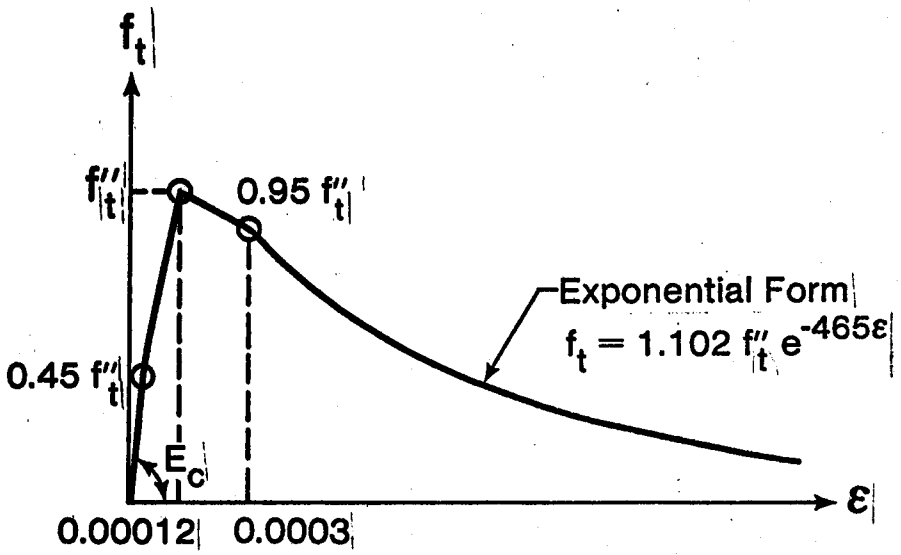

Figure 3.8 - Proposed Tensile Stress-Strain Curve for Concrete

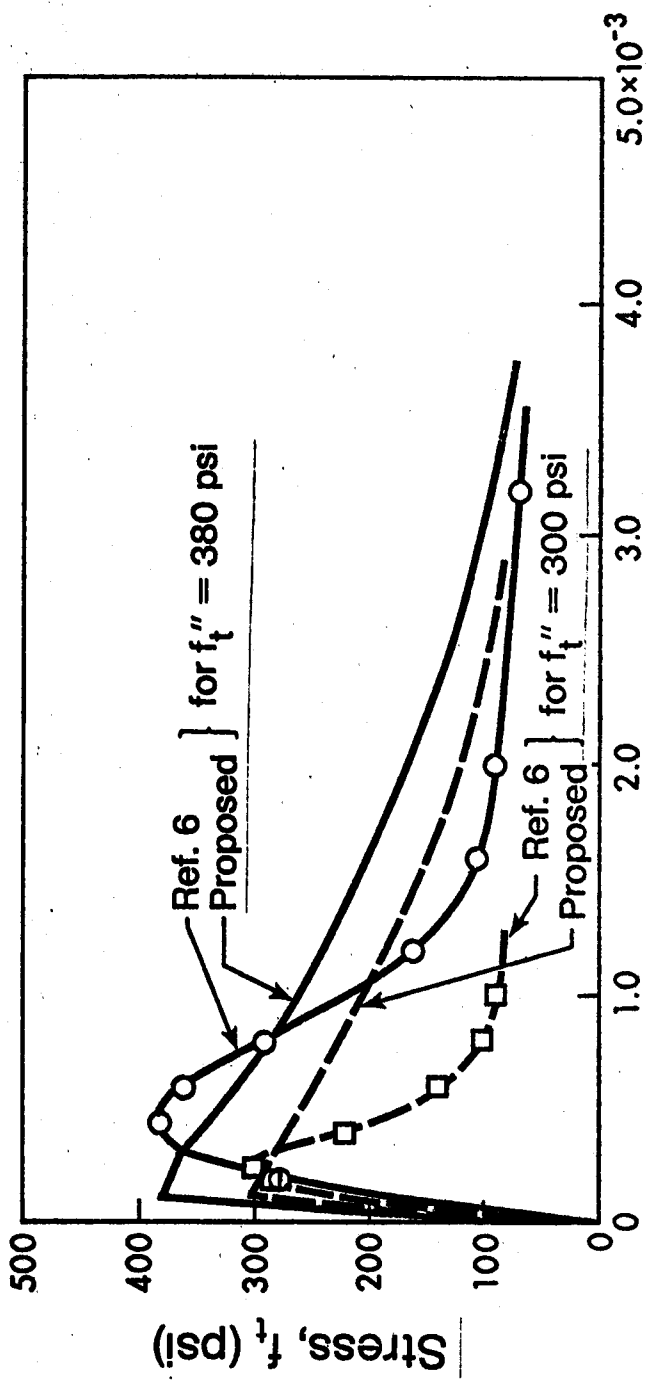

Figure 3.9 - Sample Comparison Between Analytical and Experimental Tensile Stress-Strain Curves for Concrete.

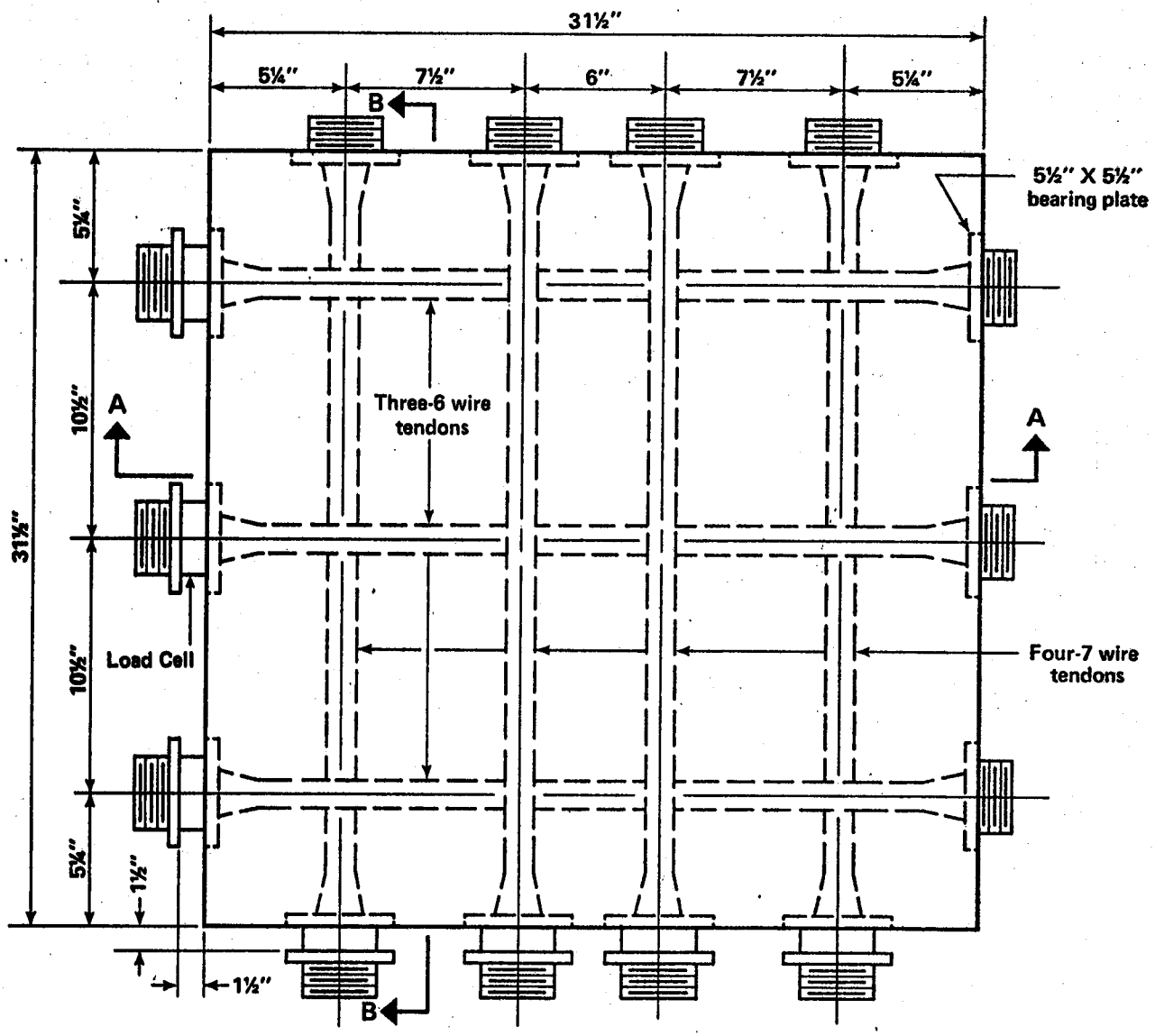

Figure 4.1 - Wall Segment Dimensions

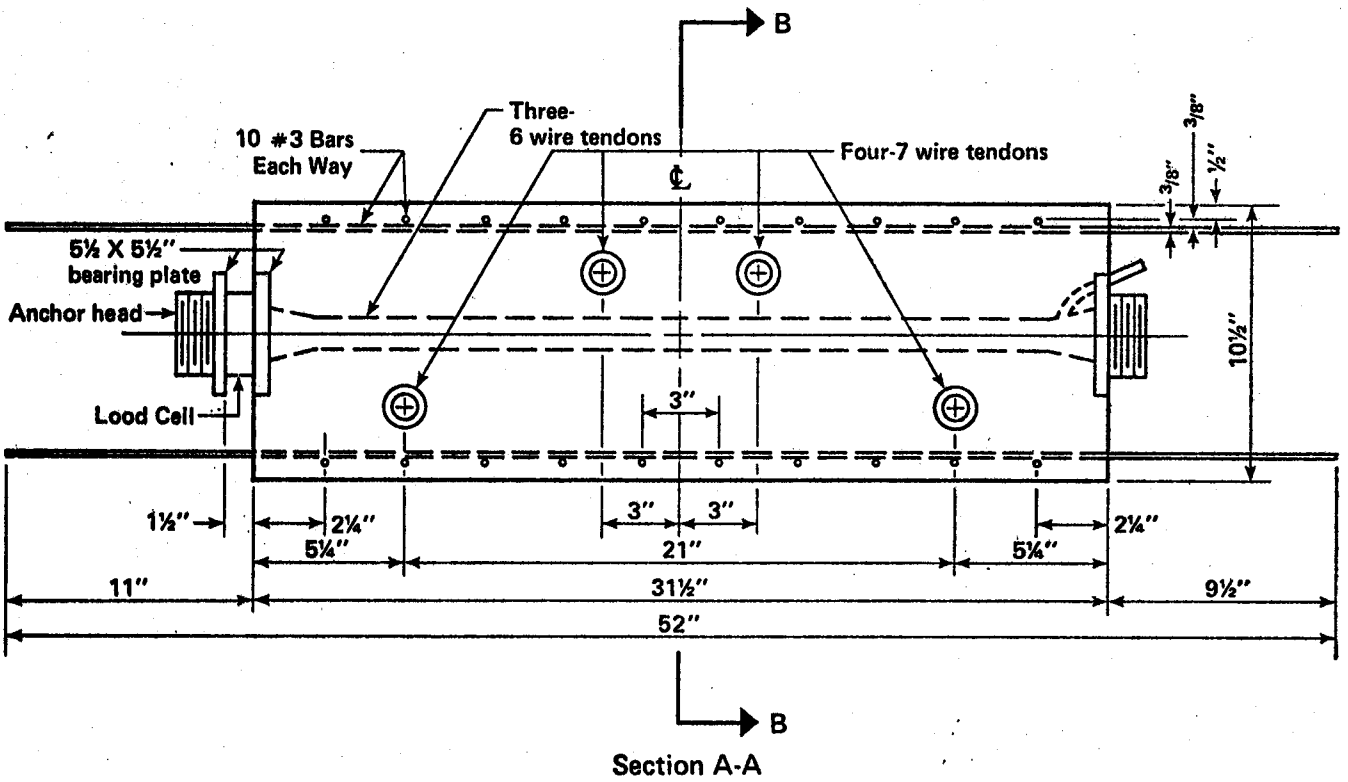

Figure 4.2 - Typical Section A-A Through Wall Segment

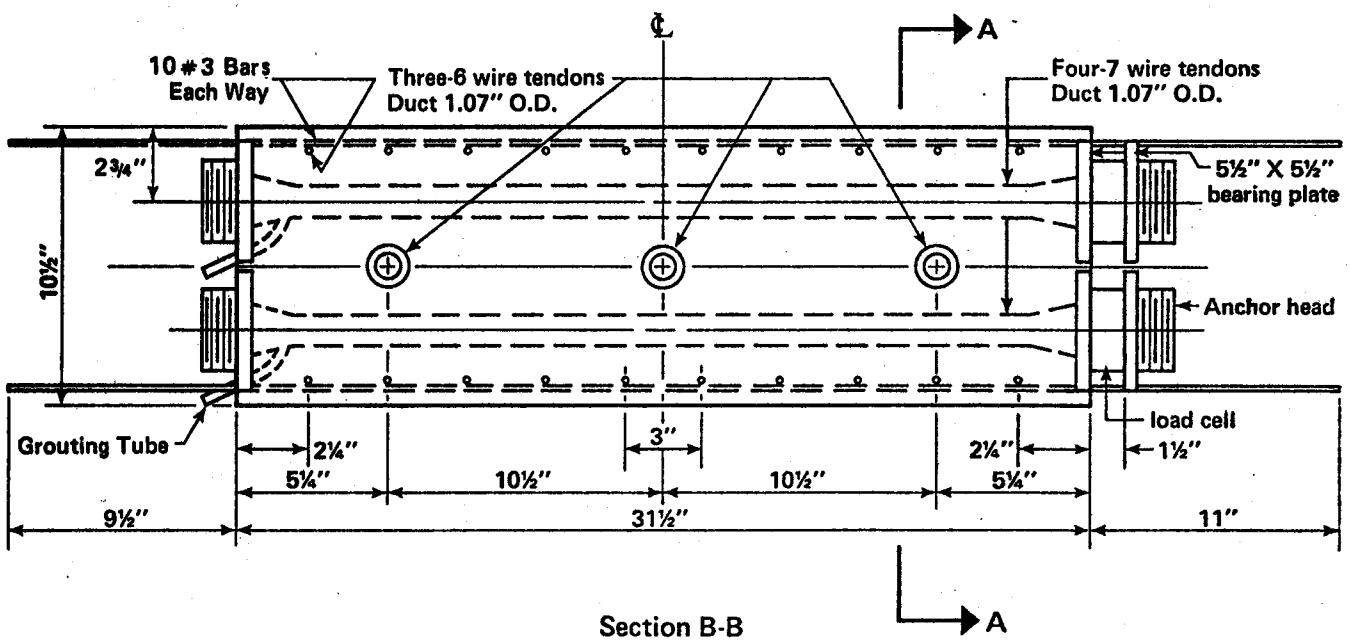

Figure 4.3 - Typical Section B-B Through Wall Segment

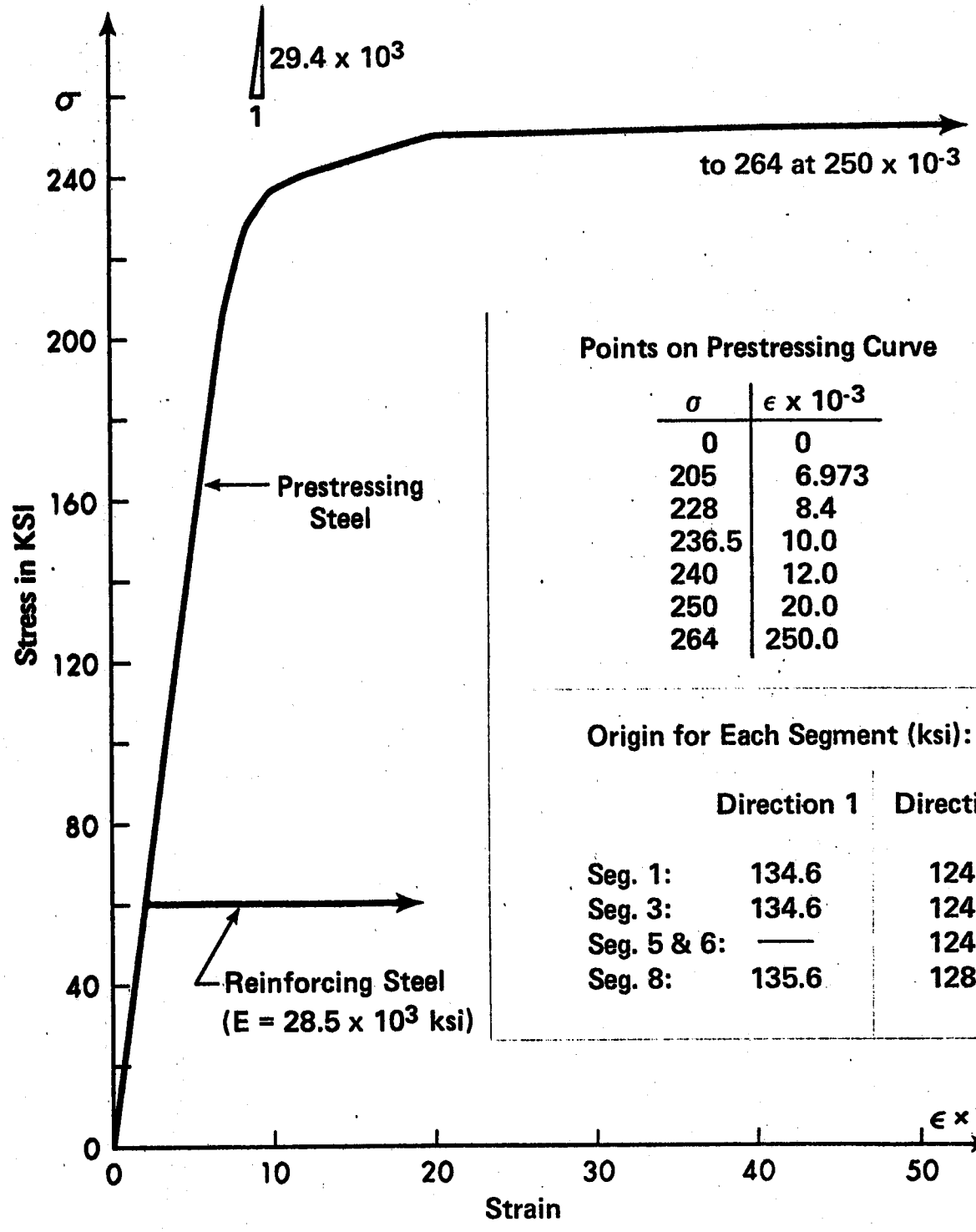

Points on Prestressing Curve

σ	$\epsilon \times 10^{-3}$
0	0
205	6.973
228	8.4
236.5	10.0
240	12.0
250	20.0
264	250.0

Origin for Each Segment (ksi):

	Direction 1	Direction 2
Seg. 1:	134.6	124.2
Seg. 3:	134.6	124.2
Seg. 5 & 6:	—	124.0
Seg. 8:	135.6	128.9

Figure 4.4 - Steel Properties for Segment Test

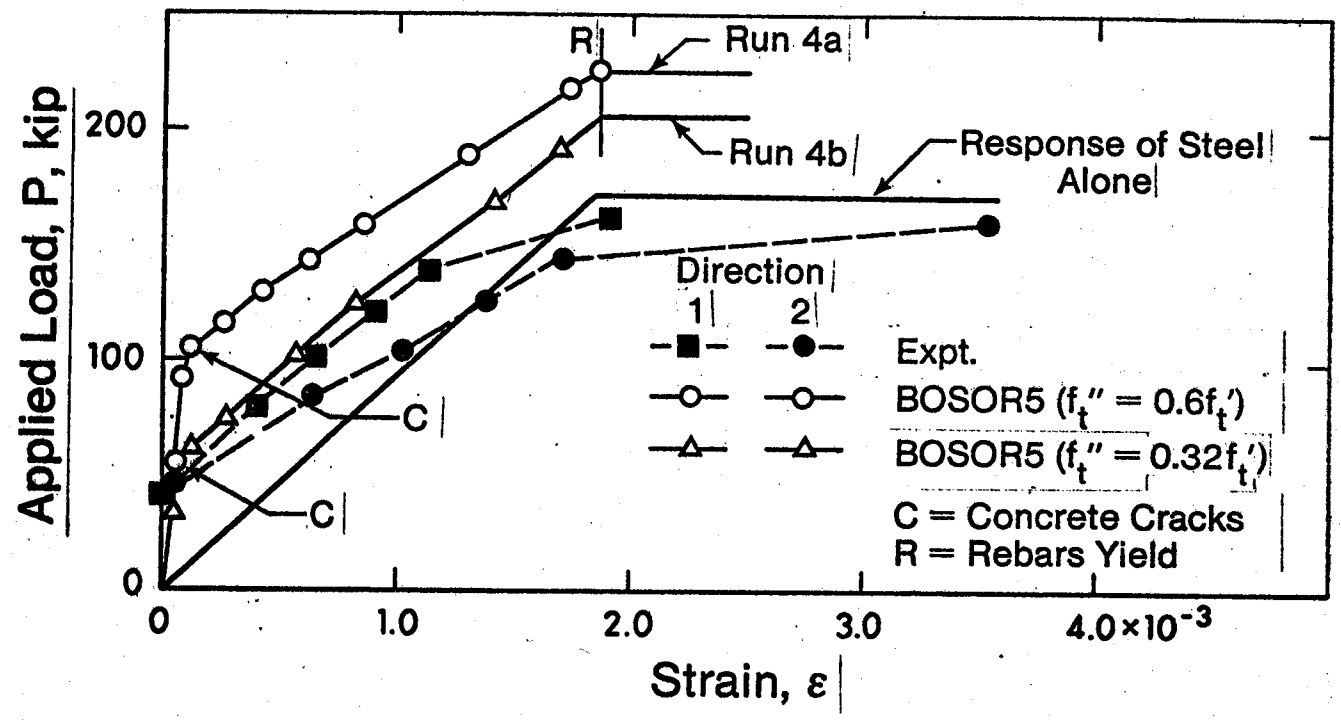

Figure 4.5 - Load-Strain Response of Segment 4.

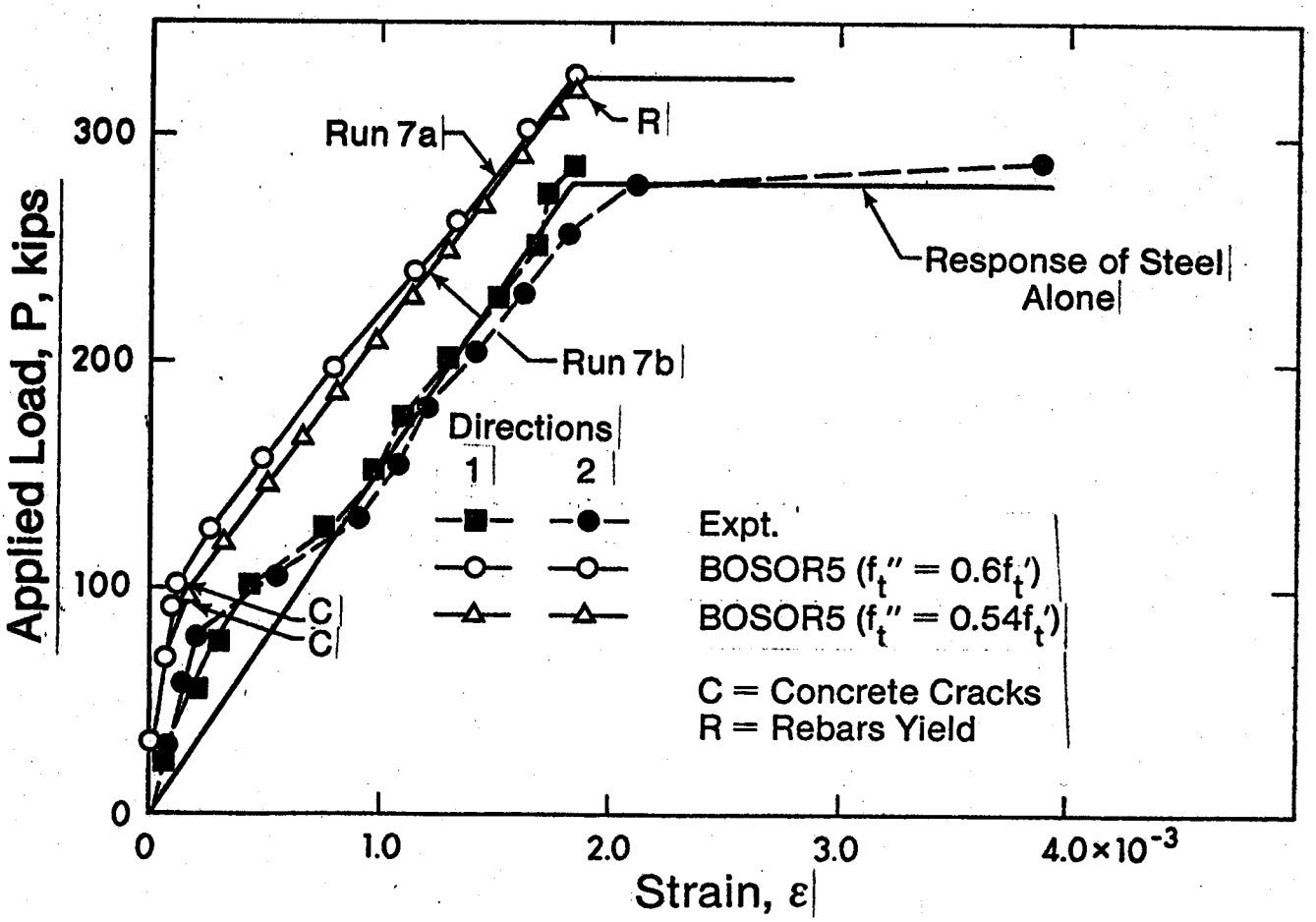

Figure 4.6 - Load-Strain Response of Segment 7.

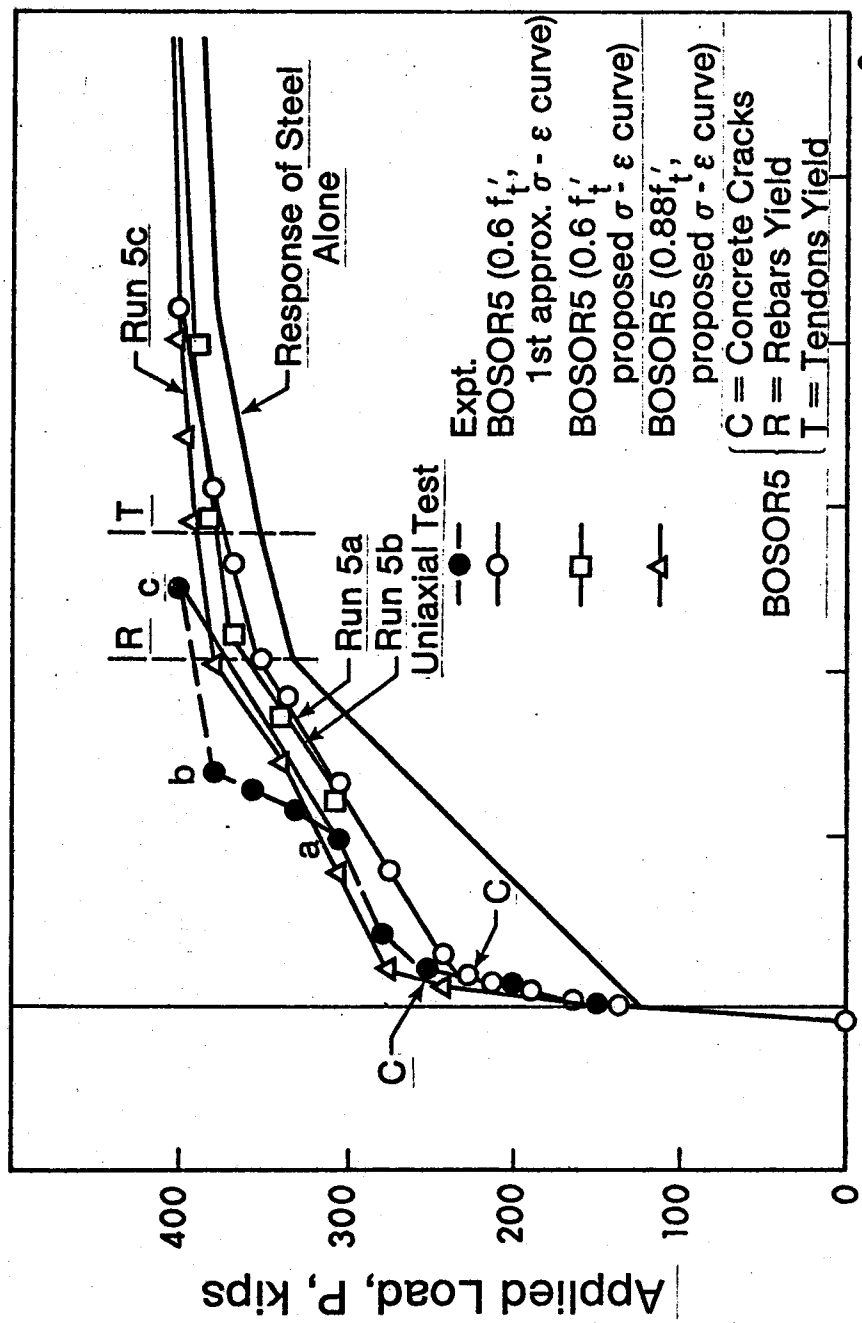

Figure 4.7 - Load-Strain Response of Segment 5.

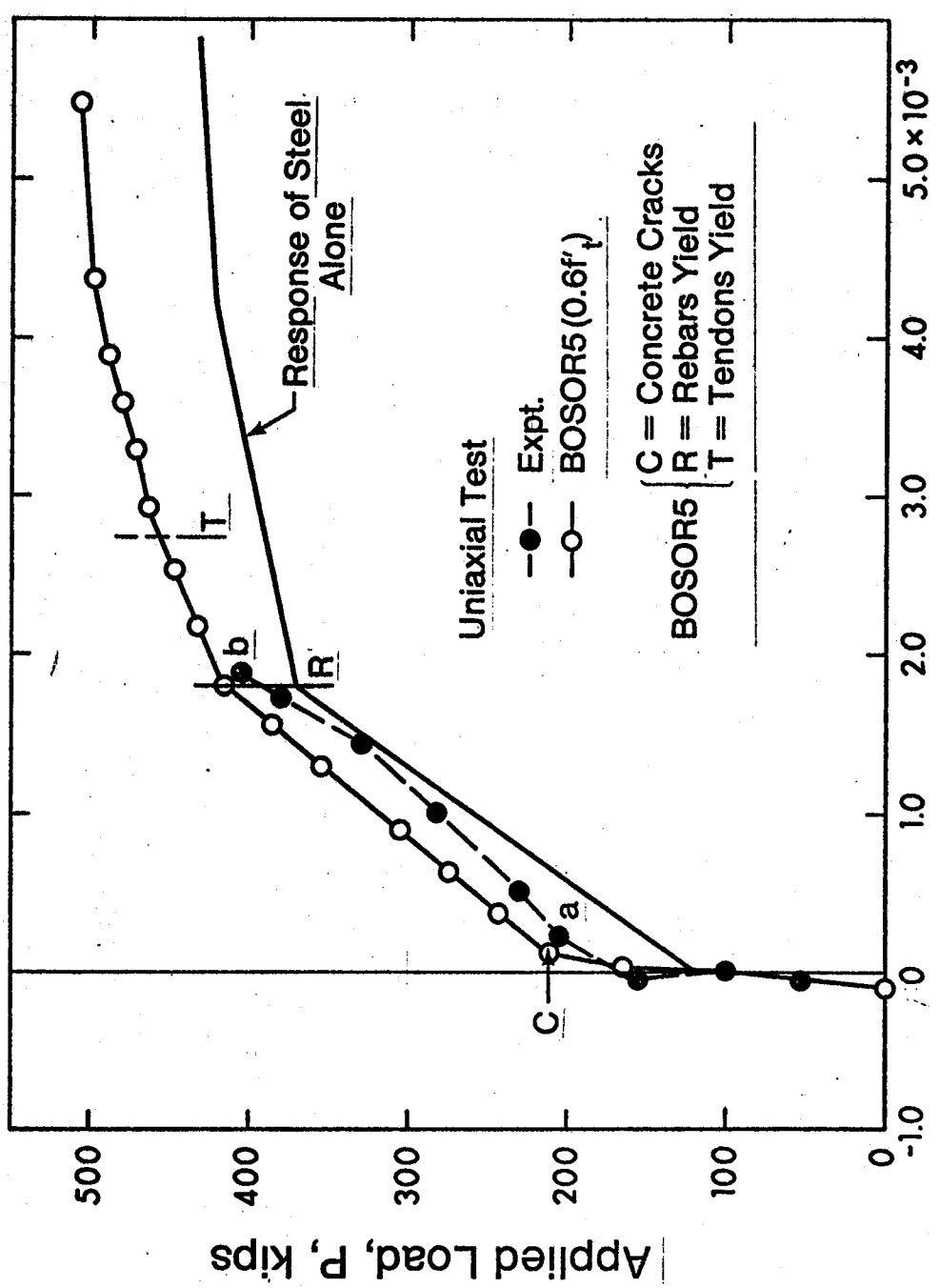

Figure 4.8 - Load-Strain Response of Segment 6.

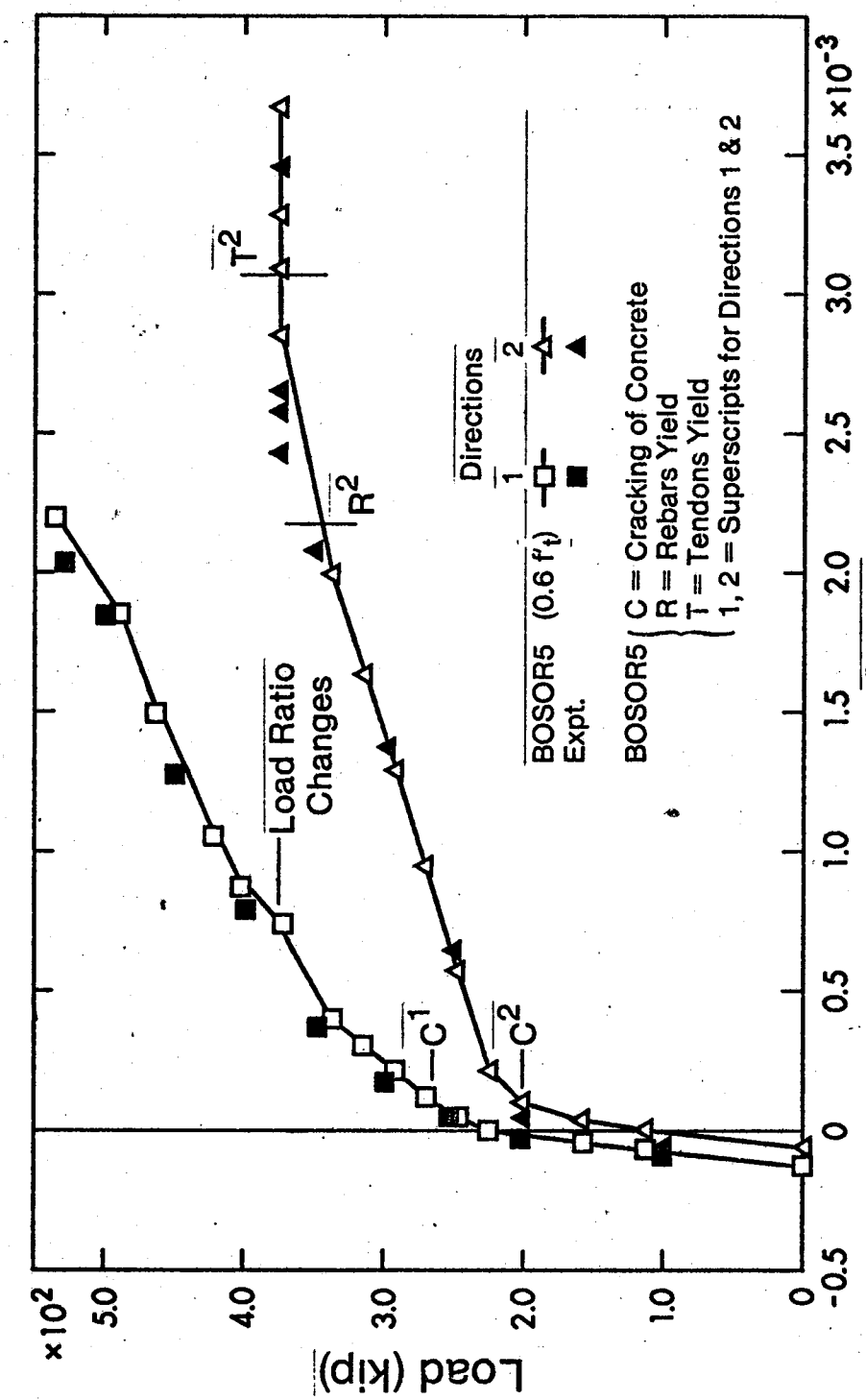

Figure 4.9 - Load-Strain Response of Segment 3

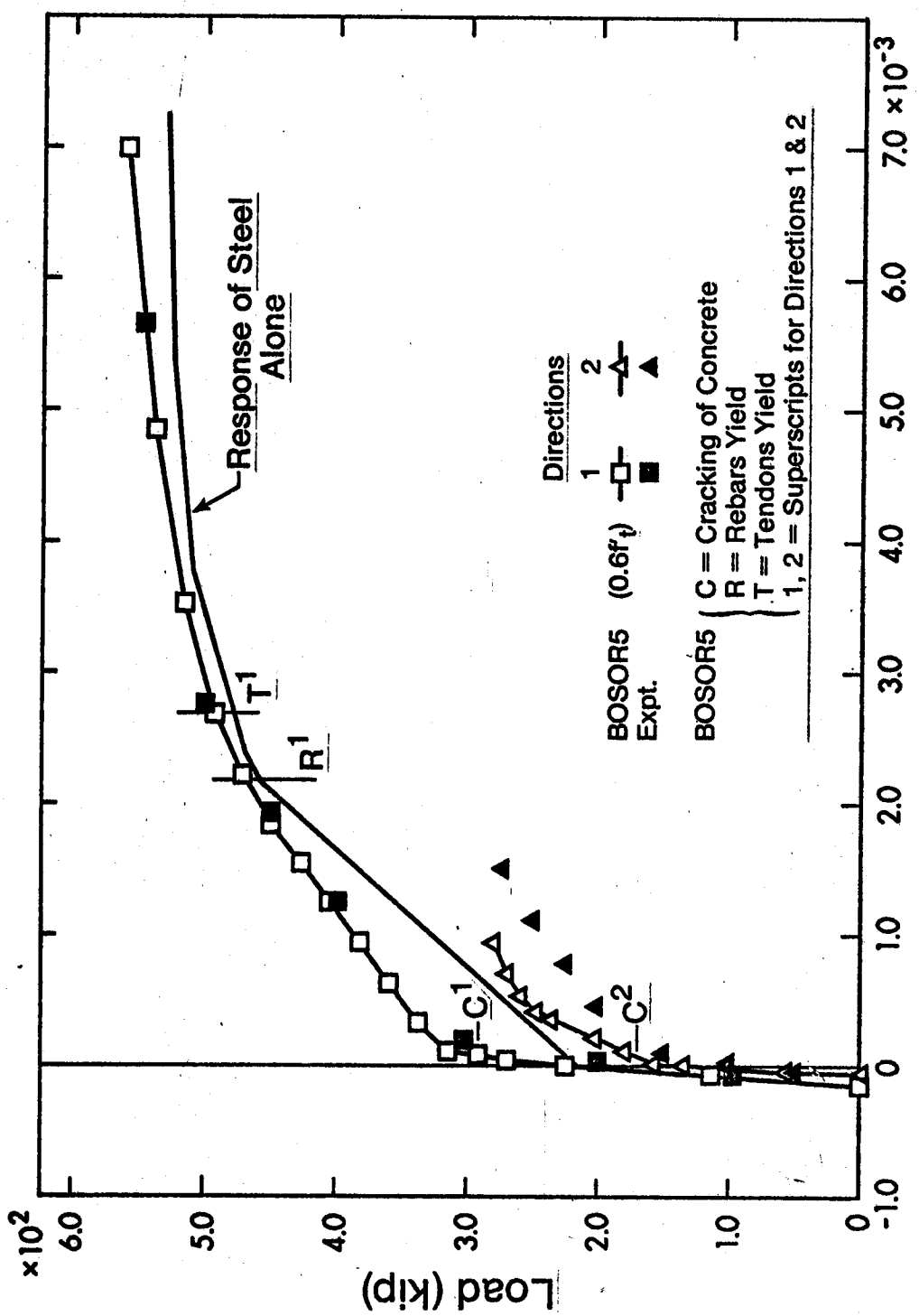

Figure 4.10 - Load-Strain Response of Segment 1

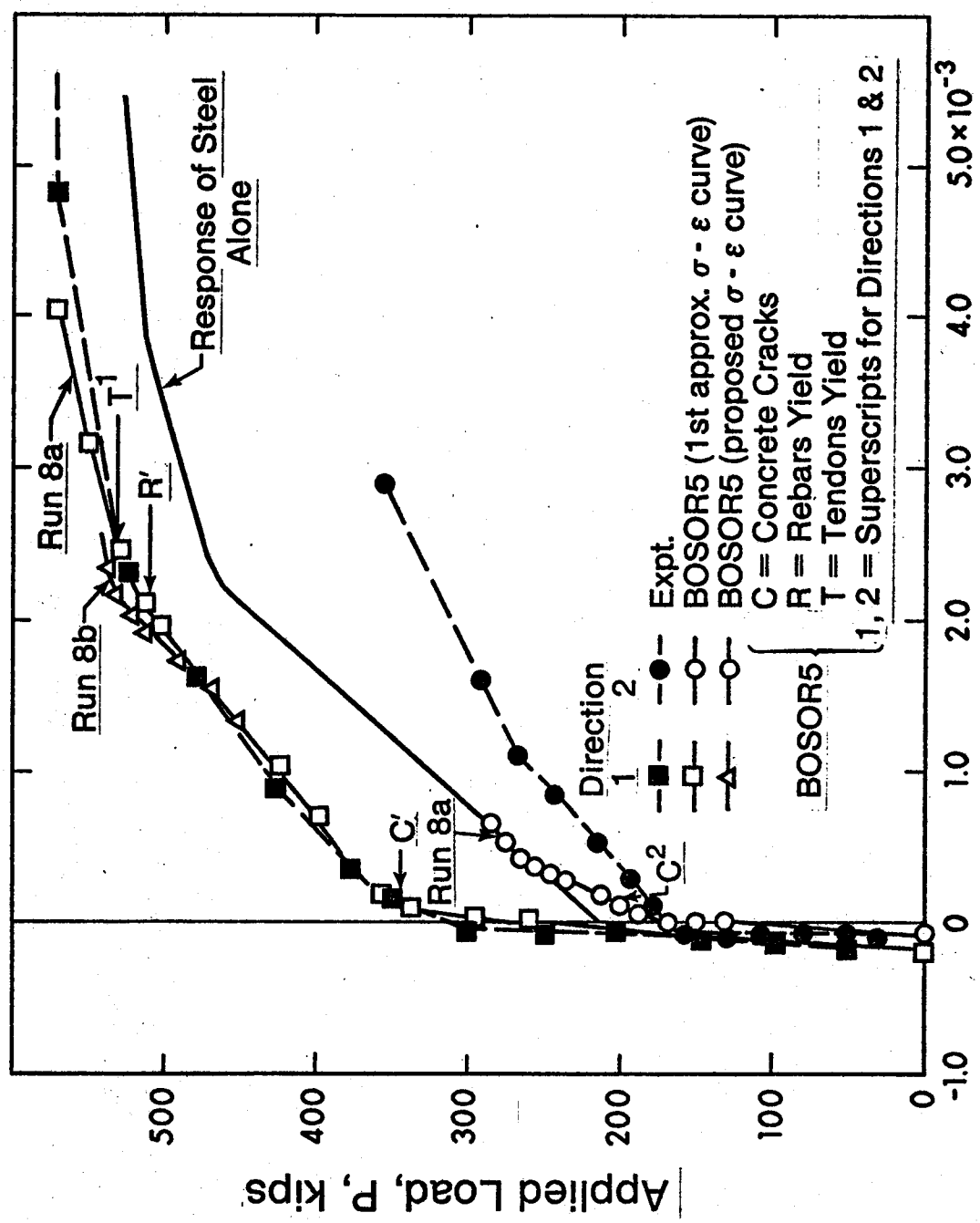

Figure 4.11 - Load-Strain Response of Segment 8.

Appendix A

Appendix A

Consistent Derivation of Uniaxial Tensile Stress-Strain Curve

A1. Introduction to Appendix A

The deduction of an effective tensile stress-strain curve from biaxially loaded test specimen data was discussed in Sect. 2.2. The technique used in the body of the report is that described in Sect. 2.2b and, except for a contribution to elastic strain, makes no effort to account for events occurring the direction orthogonal to the maximum strain. It would, however, be possible to derive an effective uniaxial curve that is consistent with the theory of Ref. 14 and utilizes the strain measurements in both directions. In view of the scatter in test results it may be questionable whether the effort expended would be worth the improvement in consistency that might arise in the shape of the derived effective stress-strain curve. However, the principal reason that the more sophisticated treatment described in the following was not pursued was that the project sponsors did not believe it to be warranted at the time of processing the results. Nevertheless, it is felt that a technique of carrying out such data reduction is at least worth mentioning in case it might be found worthwhile at some later date.

A2. Basis for Consistent Derivation

The concept of Ref. 14 is to relate the effective plastic strain to a uniaxial response curve. For a stress path following along the tensile σ_1 axis in biaxial space, the theory of Ref. 14 would yield

$$\dot{\varepsilon}_{ul} = \frac{\dot{\sigma}_1}{E} + \dot{\varepsilon}^P_{ul} \qquad A.1$$

But

$$\{\dot{\varepsilon}^P\} = \{B\}\dot{\bar{\varepsilon}}^P/B \qquad A.2$$

and since ; for a uniaxial path,

$$\{B\} = \begin{Bmatrix}1\\0\end{Bmatrix} \qquad A.3$$

we have

$$\dot{\varepsilon}^P_{ul} = \dot{\bar{\varepsilon}}^P \qquad A.4$$

Also,

$$\dot{\mu}_1 = \beta_1 \dot{\bar{\varepsilon}}^P \qquad A.5$$

and since $\beta_1 = 1$ for the uniaxial path, we have

$$\dot{\mu}_1 = \dot{\varepsilon}^P_{ul} \qquad A.6$$

Substituting A.6 into A.1 and integrating yields

$$\varepsilon_{ul} = \frac{\sigma_1}{E} + \mu_1 \qquad A.7$$

in which μ_1 identifies with the plastic strain in direction 1.

Now in a biaxial test the biaxial force vector $\{P\}$ is imposed and the resulting total strain vector $\{\varepsilon\}$ is measured. By the technique of Sect. 2.2b the biaxial force vector may be converted to a biaxial stress vector $\{\sigma\}$, and the plastic strains associated with any experimental point may then be computed as

$$\{\varepsilon^P\} = \{\varepsilon\} - [D]^{-1} \{\sigma\} . \qquad \text{A.8}$$

Hence the plastic strain increments between two experimental points are

$$\{\Delta\varepsilon^P\} = \{\varepsilon^P\} - \{\varepsilon^P\}_o \qquad \text{A.9}$$

where the subscript o indicates the previous experimental point.

Since the stress points $\{\sigma\}$ and $\{\sigma\}_o$ are expected to be on the yield curves, we have

$$\{\Delta\mu\} = \begin{Bmatrix} \beta_1 \\ \beta_2 \end{Bmatrix} \Delta\bar{\varepsilon}^P \qquad \text{A.10a}$$

$$= \begin{Bmatrix} \beta_1 \\ \beta_2 \end{Bmatrix} \sqrt{\langle\Delta\varepsilon^P\rangle \{\Delta\varepsilon^P\}} \qquad \text{A.10b}$$

Hence the equivalent uniaxial strains in the two directions may be computed, for the stress point, as

$$\begin{Bmatrix} \varepsilon_{u1} \\ \varepsilon_{u1} \end{Bmatrix} = \frac{1}{E} \begin{Bmatrix} \sigma_{t1} \\ \sigma_{t2} \end{Bmatrix} + \sum_{i=1}^{n} \{\Delta\mu\}_i \qquad \text{A.11}$$

where n is the number of stress increments.

Let us assume that $\mu_1 > \mu_2$, and that h' is the derivative of the hardening function with respect to μ. Then at the point $\{\sigma\}$,

it is necessary that

$$F(\{\sigma\}, \sigma_c, \sigma_{t10} + h'\Delta\mu_1, \sigma_{t20} + h'\Delta\mu_2) = 0 \qquad \text{A.12}$$

and this equation may be solved interatively for h'. Once h' has been determined, the σ_t values at the current point may be established as

$$\sigma_{t1} = \sigma_{t10} + h'\Delta\mu_1 \qquad \text{A.13a}$$

and

$$\sigma_{t2} = \sigma_{t20} + h'\Delta\mu_2 \qquad \text{A.13b}$$

Knowing these values, the associated strains are determined from Eq. A.11.

An effective stress-strain curve in tension then is determined by the sets of values $(\varepsilon_{u1}, \sigma_{t1})$.

It is suggested that the points $(\varepsilon_{u2}, \sigma_{t2})$ can be forced along the same curve as $(\varepsilon_{u1}, \sigma_{t1})$ by placing the proper expression for σ_{t2} into Eq. A.12. That is, if $\varepsilon_{u2}<\varepsilon_{u1}$, h' in Eq. A.13b is known because the curve at this point has already been traced by $(\varepsilon_{u1}, \sigma_{t1})$. Therefore, Eq. A.12 is solved only for the h' associated with $\Delta\mu_1$.

This procedure was not implemented for the reasons stated in Sect. A.1.

Appendix B

Appendix B

Example of the Determination of Cracking Load and Tensile Strength of Concrete

The determination of the cracking load is illustrated herein for wall test segment 1. The load at which the first cracking occurs on a face of the segment and in one of the loaded directions has been determined from the change in the slope of the load-strain relationship for that face. For example, the cracking load on Face A in direction 1 (vertical direction) has been determined as 300 kips as shown on Fig. B.1. Similarly, the determination of the cracking loads on the other face and in the different directions are shown in Figs. B.2 to B.4. These cracking loads are summarized below:

	Cracking Load (kips)
Vertical direction, face A =	300.0 (critical cracking load)
face B =	325.0
Horizontal direction,	
face A =	194.0
face B =	179.3

These are the values appearing in columns 2 to 5 of Table 3.2. Now noting that the ratio of the applied vertical load to the horizontal load is 2:1, the 'lowest' load level at which cracking first occurs is 300:150, that is, on face A in the vertical direction. Hence this number is underlined in Table 3.2.

To calculate the moment induced by the loading system, it is assumed such moment is primarily caused by the force differential $(P_1 - P_2)$ between the rebars, as shown in Fig. B.5. The forces in the horizontal strands do not induce any moment in the horizontal direction because they are centrally located. The forces in the vertical strands are assumed to be concentric because they can be accurately adjusted at the start of the test. Hence, the applied moment, M, is

$$M = (P_1 - P_2)\, a \qquad \text{B.1}$$

where a is the lever arm of the rebars. A similar moment is calculated at the other end of the segment and the average, M_{av}, of the two moments is then used for computing the tensile strength f''_t as follows,

$$f''_t = \frac{P}{A_t} \pm \frac{M_{av}}{Z_t} - f_{pc} \qquad \text{B.2}$$

where P is the total applied load at the time of cracking; A_t is the transformed uncracked section area; Z_t is the transformed section modulus; and f_{pc} is the compressive stress in the concrete due to the effective prestress after all losses have occurred. The values of P_1 and P_2 are obtained from the electrical strain gages located on the rebars as shown in Fig. B.5, whereas P is obtained directly from the loading machine. For Segment 1 the important data are,

$P = 300.0$ kips

$a = 4.5625$ in.

$f_{pc} = 676.2$ psi

$A_t = 354.91$ in.^{2}

$Z_t = 645.8$ in.^{3}

P_1 = 33.76 kip
P_2 = 12.91 kip
} one end

P_1 = 26.84 kip
P_2 = 8.64 kip
} the other end

The average moment at the load level of 300 kips is,

$$M_{av} = \frac{(33.76 - 12.91)\ 4.5625 + (26.84 - 8.64)\ 4.5625}{2} = 89.12 \text{ k.in.}$$

The tensile strength of concrete is,

$$f''_t = \frac{300.0 \times 10^3}{354.91} + \frac{89.12 \times 10^3}{645.8} - 676.2$$

$$= 845.3 + 137.9 - 676.2$$

$$= 307.0 \text{ psi}$$

This number appears in column 7 of Table 3.3 for Segment 1.

If the bending effect is ignored, the cracking load is obtained from the plot of the vertical load against the average strain of faces A and B. The cracking load is 320 kip in the vertical direction as determined from Fig. B.6 and is 179.3 kip in the horizontal direction as determined from Fig. B7. Because of the 2:1 load ratio, the former value is then the critical value and the average tensile strength is,

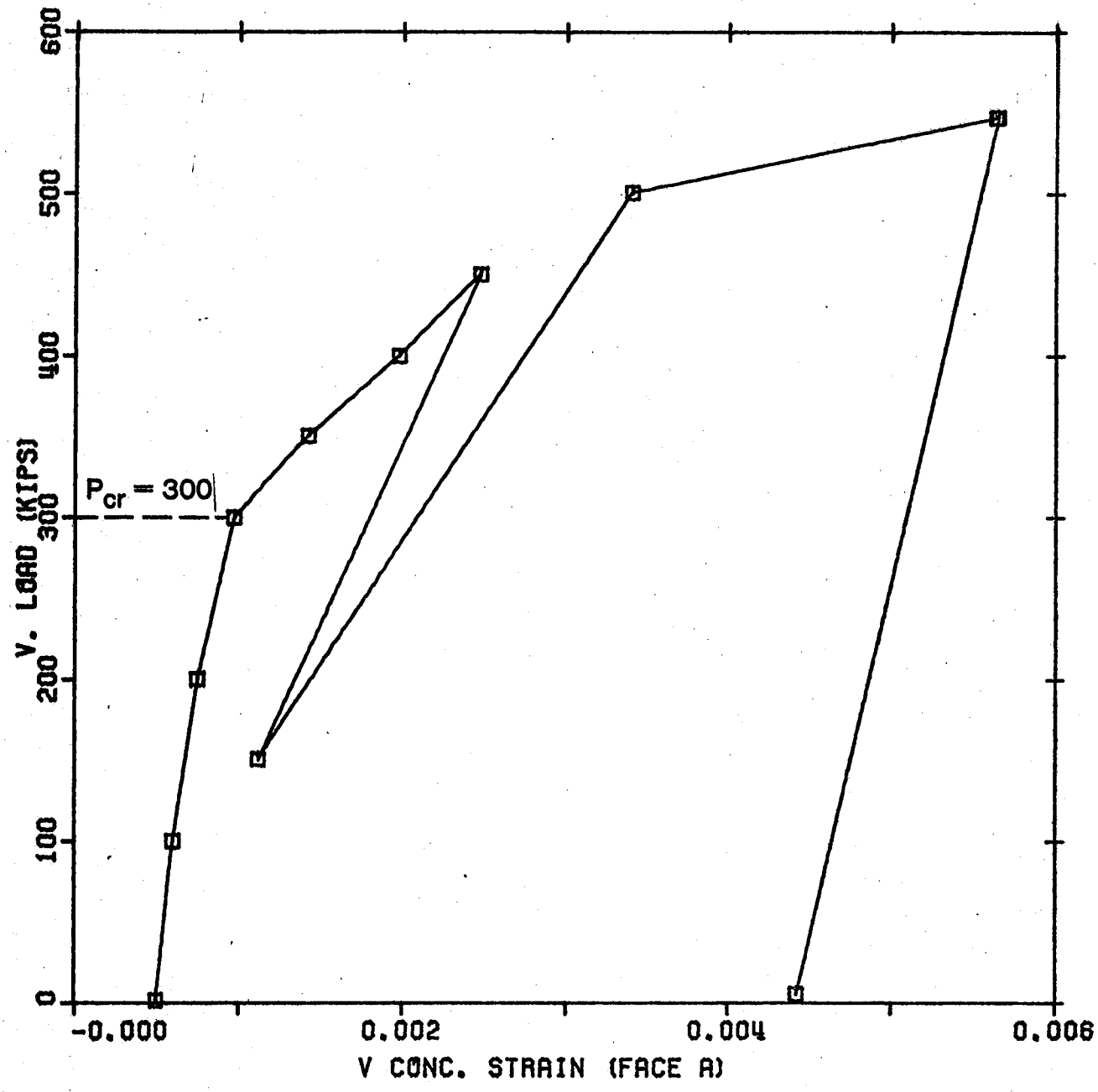

Figure B.1 Vertical Strains on Face A of Segment 1

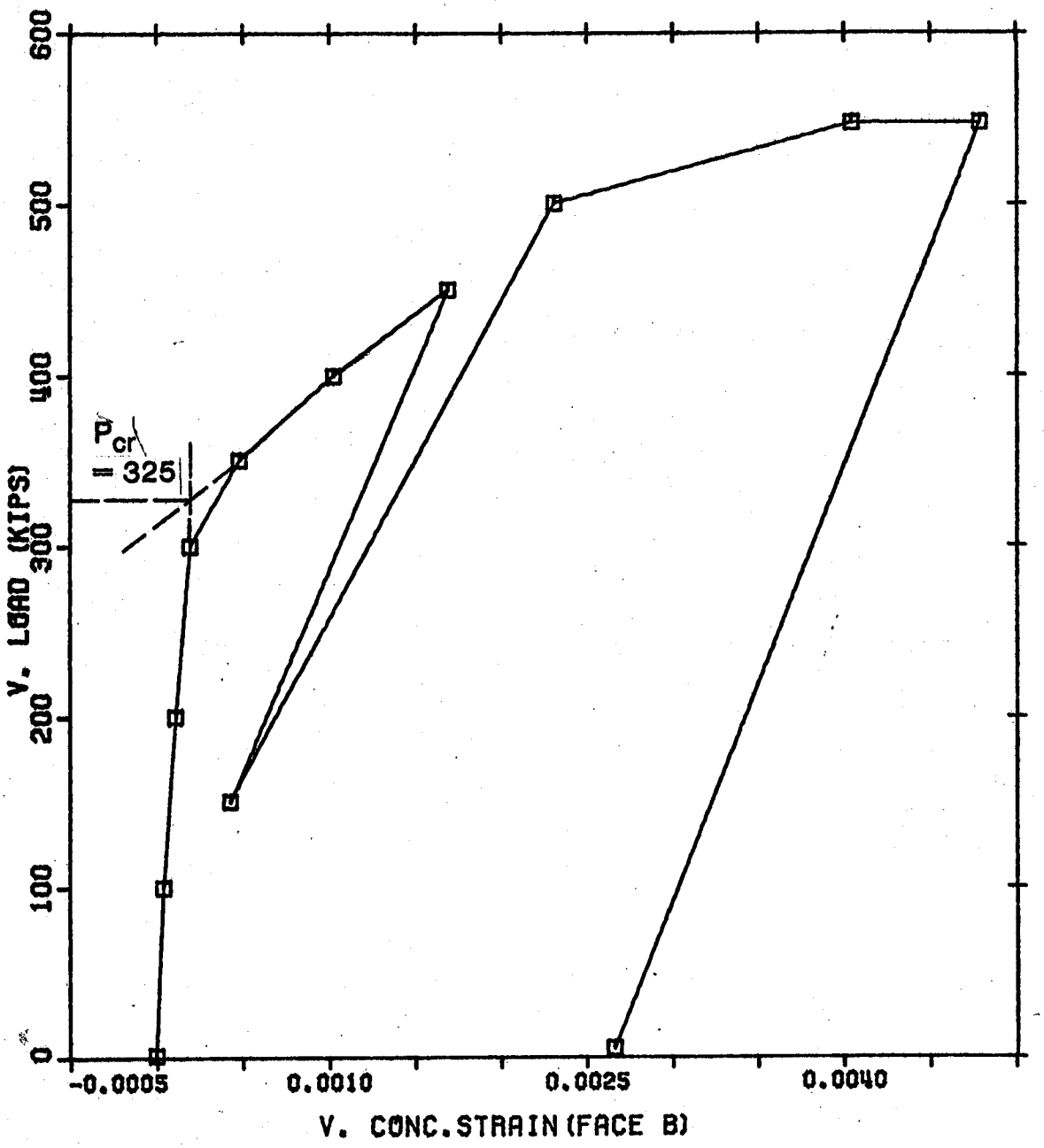

Figure B.2 Vertical Strains on Face B of Segment 1

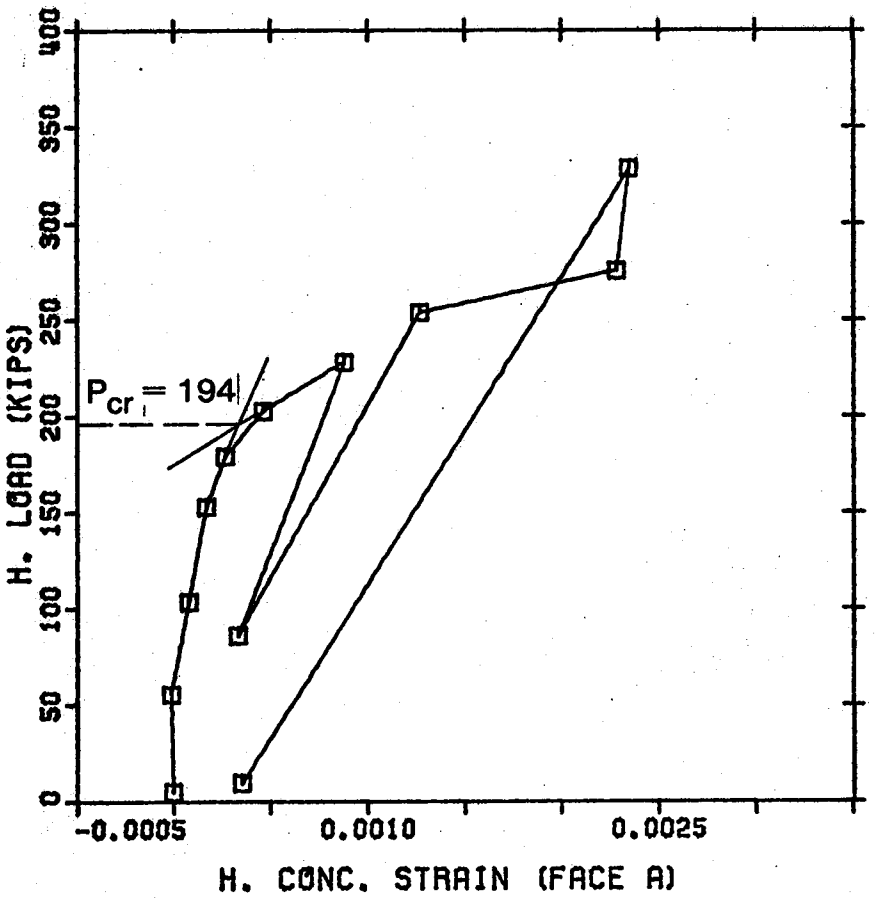

Figure B.3 Horizontal Strains on Face A of Segment 1

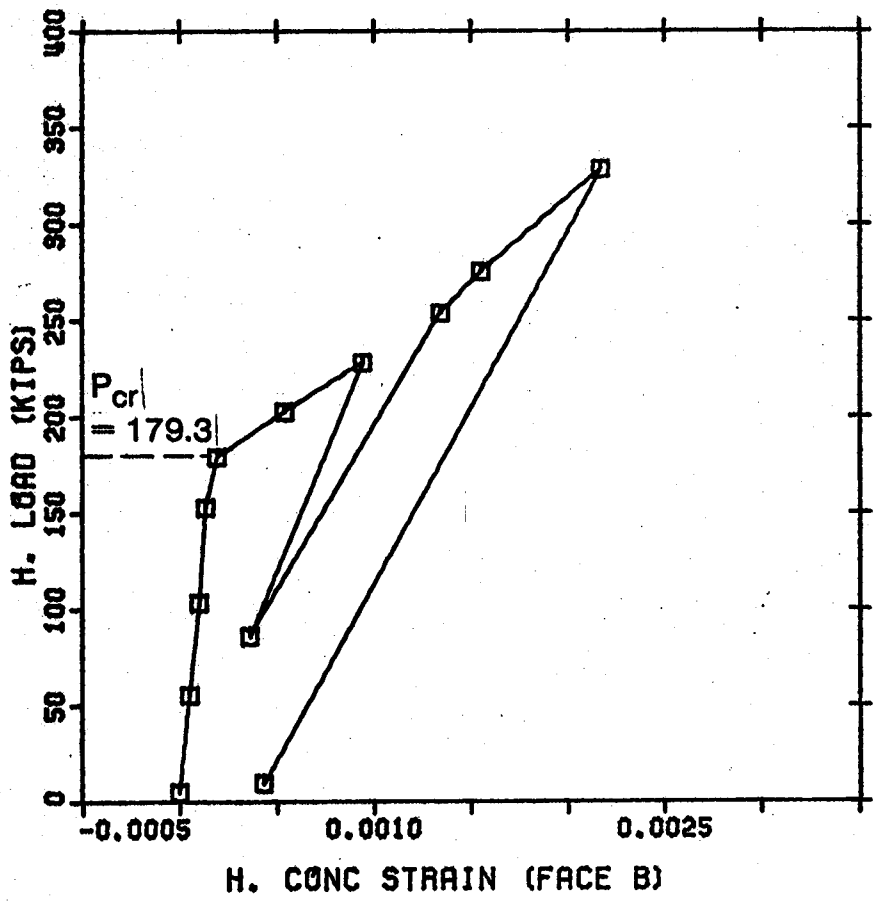

Figure B.4 Horizontal Strains on Face B of Segment 1

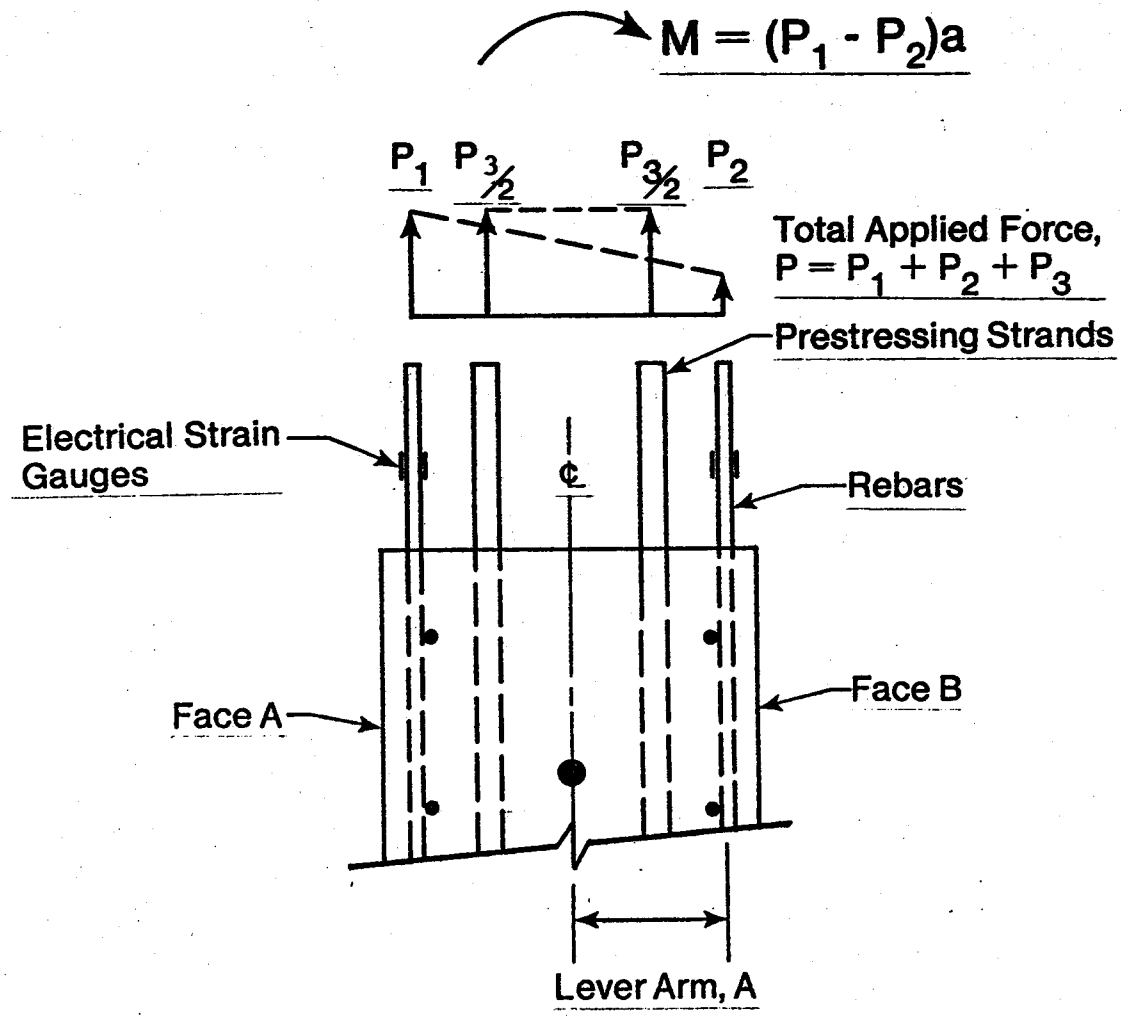

Figure B.5 - Partial Vertical Section Through Wall Segment

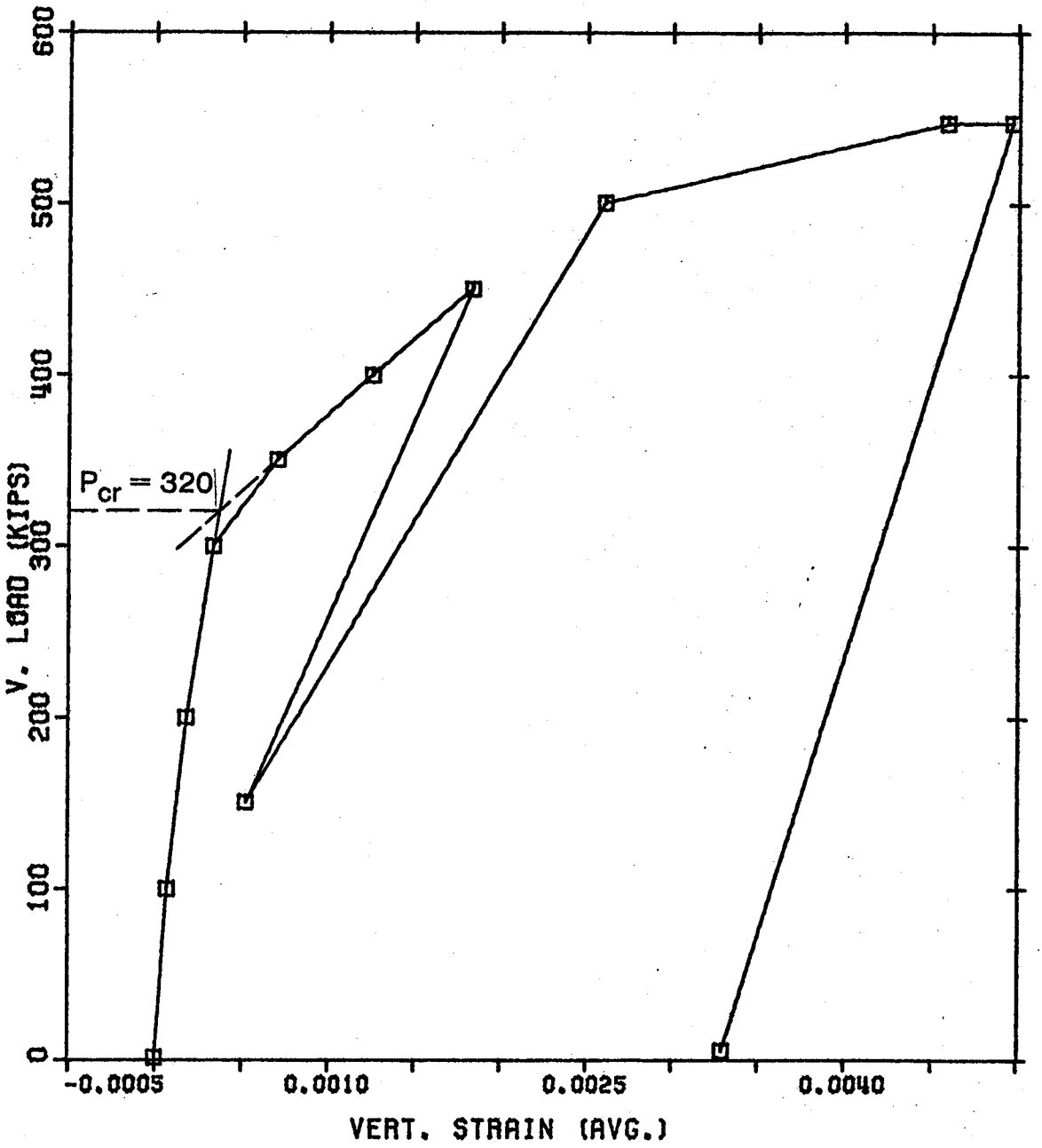

Figure B.6 Average Vertical Strains of Segment 1

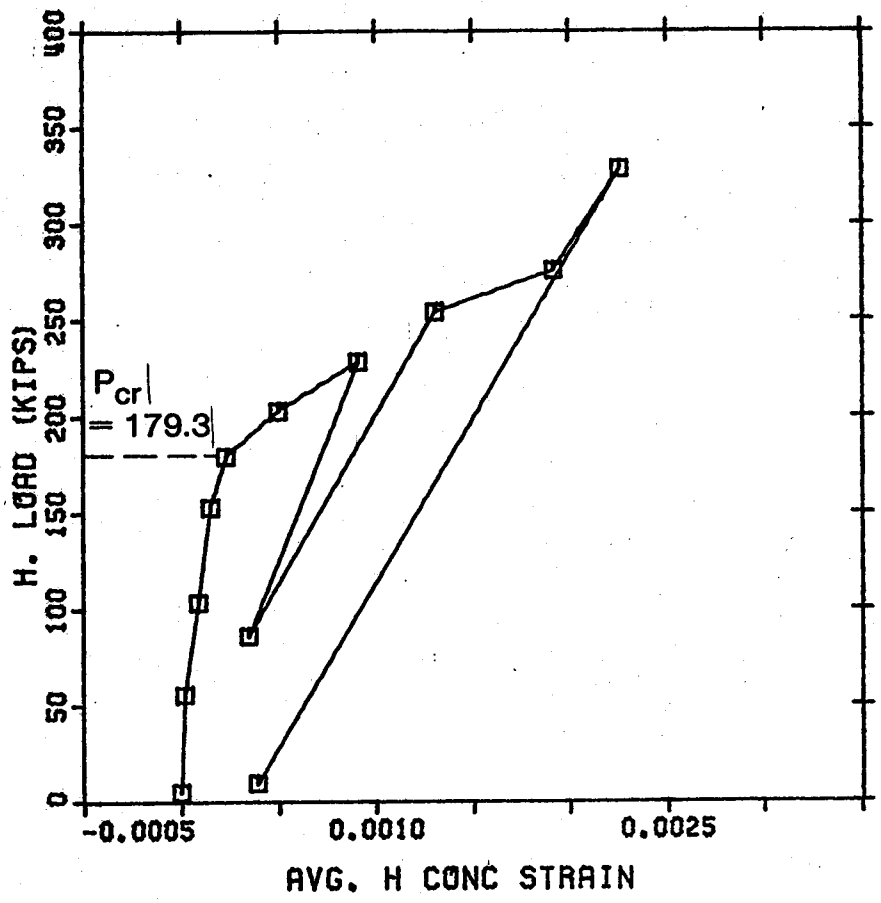

Figure B.7 Average Horizontal Strains of Segment 1